Instrumentation Development, Measurement and Performance Evaluation of Environmental Technologies

Quarterly Technical Progress Report
for the period
April 1, 2001 - June 30, 2001

Dr. John Plodinec, Principal Investigator

Report No. 40395R12

Prepared for the U.S. Department of Energy
Agreement No. DE-FC26-98FT40395

Diagnostic Instrumentation and Analysis Laboratory
Mississippi State University
205 Research Boulevard
Starkville, Mississippi 39759-9734

dial@dial.msstate.edu
www.msstate.edu/Dept/DIAL

Notice

Table of Contents

List of Figures

List of Tables

Executive Summary

Characterization of Heavy Metals and Radionuclides

On-line isotopic analytical system for uranium and other actinides. Isotopic resolution for uranium was obtained for the first time using CRDS. The 286.6, 358.4 and 409-nm transitions have been isotopically resolved, yielding detection limits of approximately 140, 300 and 230 ppb respectively for U-235. The U-238 detection limit is slightly higher (600 ppb) for the 286.6-nm line because of a small background absorption line in the plasma. Detection of U-235 at its natural abundance level (0.7%) was demonstrated as well using a U-235 concentration of 1.25 ppm and the 286.6-nm transition. Although experiments aimed at evaluating system performance for the 424-nm transition were initiated, defective mirrors have delayed this work temporarily.

In searching for an ideal pair that combines a large isotopic separation with high transition probability and high lower-state population, we investigated a number of excitation/fluorescence transition pairs for LIF. For the 286.6/288.9-nm pair, isotopically resolved LIF excitation spectra yielded a detection limit of approximately 150 ppb for both U-235 and U-238. The other two pairs studied, with excitation/fluorescence transitions at 573.4/393.2 nm and 409.0/385.9 nm,

respectively, exhibited either low detection sensitivity or small isotopic separation.

Using transition metals, we have evaluated large-volume injection methods for ion chromatography with UV/VIS detection of a post-column derivative. Detection limits of 10 ppb were demonstrated with a 2-mL injection without pre-concentration. Oxalic acid was used as the mobile phase, and PAR (a resorcinol salt) was used as the post column agent. No excess band broadening or other poor peak characteristics were observed with large volume injections to 100 ppb. Poor peak shape was evident at 10-ppm concentrations.

Laser probe for technetium monitor. To evaluate the signal-enhancing technique that uses a magnetic field to confine the laser-induced plasma, LIBS spectra of various elements such as Mn, Mg, Cr, and Ti were recorded in the absence and presence of a magnetic field. The analyses of these data show that the LIBS signal is enhanced approximately two times in the presence of a magnetic field. This ultimately decreases the limit of detection (LOD) for these tested elements by a factor of half. The LIBS spectra of iron in liquid solution in the presence of a magnetic field was also recorded, showing that the line emission signal was enhanced by nearly three times when the concentration was below 10 ppm. The background emission decreases such that line emission becomes dominant. We were able to record the LIBS spectra of 10-ppb iron in liquid solution with the help of jet and magnetic field arrangements.

Development of Tools for Long-term Monitoring

Monitoring plant physiological status in contaminated environments by high-resolution spectral imaging. During this quarter, we have performed an extensive literature survey to determine a variety of plants that could be potential accumulators/hyper accumulators for selected heavy metals. After consultation with plant scientists, we have

selected two plants (*brassica juncea* and barley) for our initial study to observe spectral signatures for metal uptake by plants. A graduate student with expertise in agriculture and remote sensing has been recruited to work on this project. A dedicated portable spectroradiometer system was ordered and received during this quarter. Planting and monitoring will begin during the next reporting period. Contact with SRS researchers interested in applying this technique to their site was made at a DOE Long Term Monitoring Workshop in Orlando; this collaboration is being pursued.

Moisture fiber-optic diode laser sensor. The aim of this project is to achieve a fiber optic relative humidity sensor. Initially, the sensor realized using a swellable hydrogel. The hydrogel was used to produce microbends in fiber, which produces loss in fiber output. The sensor realized using the micro-bending phenomenon based on hydrogel works in principle but was found to react slowly. The evanescent wave-absorption phenomenon was then applied, and at present we are able to obtain a fast- responding relative-humidity sensor, which can effectively sense relative humidity above 78 percent.

Application of imaging techniques. Development of DIAL's Fourier transform profilometry (FTP) system has continued. The phase shift extraction process has been improved by replacing the usage of a one-dimensional fast Fourier transform (1D-FFT) that was used on a line of pixels within an acquired image (with subsequent line-by-line processing to construct the phase shift map for the whole image). The phase shift extraction analysis software has been modified by replacing the 1D-FFT module with a 2D-FFT module. This modification yields a better representation of the phase shift map for the whole image. Also, for the final surface profile, a user-predefined median filter was integrated into the analysis system to smooth the height spikes that generally result from errors introduced during data acquisition and the preceding analysis phases. Integration of a higher-resolution camera (for increasing the target sampling frequency) into the current system is continuing. Modification of the current system

packages for the newly installed imaging system drivers is also underway.

In an effort to expand thermal imaging's spectral response region, a near-infrared (NIR) camera system has been obtained. Characterization of the NIR camera's baseline parameters has begun. Parameters include the bad-pixel map and the dark-current pixel intensity map in the InGaAs focal plane array. An image bad-pixel correction mask has been established for future on-line acquired image correction. A study of the image file format [Portable Network Graphics (PNG)] was initiated. The PNG file format is used for loss less compression of images acquired from DIAL's non-eight-bit monochrome cameras. In support of the RIC-AVS project, the thermal imaging systems were used to monitor a batch-melting process. The melt surface temperature map is provided to the system operator in near-real time. A new version of the imaging system drivers has been installed. Modification of current system packages has been completed for the thermal imaging system.

Significant progress has been made toward the development of a computerized spectral imaging system. The system has been tested in our laboratory for real-time spectral image acquisition. This development effort included the integration of image collection and analysis in a single computer program. The system has been tested by recording 307-nm spectral images of OH emission in an ICP plasma. Additional modifications enable the software to properly synchronize data acquisition of spectral images with our pulsed laser.

The information-sifting effort has concentrated on locating spectral and image libraries that will aid in the analysis of spectral images as well as diffuse reflectance spectra. The images and data will be generated as part of the off-line melter inspection effort and the plant monitoring effort. Development of a search engine for use with these libraries has begun.

Hanford Tank Waste Chemistry

Saltcake dissolution. Additional simulations were performed on the BY-109 saltcake. Results obtained previously indicate that fluoride and sulfate concentrations predicted by ESP take on constant values between 100 and 150 cumulative weight percent dilutions. This result is at odds with the experimental data, and additional calculations at smaller diluent increments have confirmed the predictions. The model error has been traced to inaccurate partitioning between the NaF and Na_3FSO_4 solids. Further comparisons with solids identification studies are in progress.

Solubility data for the Na-F-SO_4-OH system, reported earlier, are being converted to a stand-alone database. Initial efforts are reported regarding the determination of the constants for the equilibrium or KFIT expression. Two different regression programs were employed. The DOS-based version, obtained form OLI, Inc., was found to provide better fits to the data than the regression tool supplied with the ESP (version 6.5) software package. Additional simulations as a function of ionic strength and temperature will provide for the incorporation of like ion interactions

Experimental data and ESP predictions are reported for the Na-F-NO_3-OH system. Measurements have been performed at 25 and 50˚C in water, 1, 3 and 5-molal hydroxide with varying levels of added nitrate. ESP predictions are in excellent agreement with the experimental results in water at 25˚C. Both fluoride and nitrate solubility decreased with added caustic, in agreement with model predictions. At both temperatures the ESP model tended to over-predict solubilities in added hydroxide. A weak temperature dependence was found for the fluoride solubility similar to that observed in the Na-F-SO_4-OH experiments reported previously. Experimental results will be subjected to regression analysis and developed into a database to improve the quality of the data called by the ESP model.

Solids formation. Results of saltwell pumping experiments with the SX-104 supernatant surrogate are presented. Process stream temperatures and pressures along with images of particle formation, agglomeration, and bed development were obtained. Particle dimensions and growth rates were similar to those determined for an earlier run at a reduced velocity or flow rate. Correlations between the experimental runs are given. Pressures and velocities were nearly super-imposable for runs with initial velocities of 15 and 8-cm/sec (flow rates of 6.8 and 3.5-gph) when plotted against reduced time. The velocity trace showed variations consistent with single particle growth, particle agglomeration and initial bed formation, moving bed flow, and plugging. The data compared favorably to models for the pressure increase as a function of bed growth and for unsteady state heat transfer. Additional experiments have been identified to further define operating envelopes where phosphate plug formation will not occur.

Details regarding further engineering tool calculations for support of slurry waste transfers at Hanford are described. Initial sensitivity calculations are being optimized to fully establish an operating envelope and allow comparisons with existing calculations performed based on the semi-empirical models currently employed. The final result of these calculations is expected to be a three-dimensional surface plot suitable for rapid operator evaluation of the success of a given transfer for a specific feed material.

Environmental Control Device Testing

Evaluation of HEPA filter performance. Work on determining the scope of work to be done in regard to HEPA filter testing and measurements continued through a number of conference calls with the NTW members. We decided to take advantage of the fact that a number of the NTW members were planning to attend the IT3 Conference in Philadelphia by scheduling a HEPA project meeting at the conference. This was a very productive meeting that helped set the goals

and scope of the project. Enough progress was made for us to begin work on a test plan for the HEPA project. Work on the test plan has already begun with some of the introductory sections being essentially finished. A first draft of some of the more technical sections of the test plan is scheduled to be sent to members of the NTW for review and comments in July. When all sections are completed and reviewed by the NTW, the test plan will be subjected to peer review by the ASME.

Process Monitoring and Control of Toxic Organics

Sampling system for dioxins, furans and other semi-volatile products of incomplete combustion and characterization. The formation of dioxins and furans during combustion processes has become a significant focus of concern over the past few years. EPA has initiated an intensive effort to characterize the different sources of dioxins in the US and to reduce the overall annual rates of emissions. The 1999 MACT for Hazardous Waste Combustors establishes an emission limit for dioxins and furans that will be technically difficult to achieve. Large strides to controlling dioxin and furan emissions from combustion processes will most easily come from an enhanced understanding of their mechanisms of formation. The work being conducted by DIAL will seek to reduce uncertainties associated with the locus of formation of these compounds and factors that contribute to their formation.

Toxic organic compound monitoring using cavity ringdown spectroscopy. The final vacuum system and pulsed valve designs for the supersonic expansion-cavity ringdown system were finalized based on the calculated gas load from the valve. Pulsed valve and vacuum components were ordered, and system construction will begin as the required components arrive. This system will initially be tested using volatile organic compounds and ultimately will be evaluated for dioxin-monitoring applications. The evaluation of the diode laser cav-

ity ringdown system for volatile organic compound detection continues using a distributed feedback diode laser. Repairs to the external cavity diode laser were necessary due to excessive mode hopping (discontinuous frequency shifts) in the laser output. This limits the wavelength tuning range and thus the sensitivity of the system, but does not prevent us from continuing to evaluate the behavior of various VOCs in the system. We continue to work to improve the reproducibility of the measurements made using this system.

TASK 1

Characterization of Heavy Metals and Radionuclides

On-line Isotopic Analytical System for Uranium and Other Actinides

D. L. Monts, Yi Su, C. B. Winstead, and Thomas Meaker

Introduction

Many DOE applications would significantly benefit from the availability of robust and convenient instrumentation for trace-level actinide monitoring and analysis. This project focuses on developing new instrumentation for on-line or at-line monitoring for actinides with isotopic analysis capability. In addition, analytical protocols for a novel concentration method for actinides are being investigated. These efforts focus on demonstrating these techniques using uranium. In addition to its value in the analytical laboratory, the combination of a simple concentration technique with a robust isotopic monitor could provide a powerful method for addressing a number of outstanding DOE needs. Potential applications include monitors for waste water and sewage treatment systems influent and effluent, and the ability to determine the isotopic content of transuranic species in low-activity waste fractions for waste classification and product acceptance. For example, the need for improved monitoring for uranium, plutonium, and americium in treatment plant influent is clearly identified in need

RF-ER11. With some additional sample pretreatment, such technology could also impact materials characterization needs by providing on-site isotopic analyses in a system that is smaller and significantly less complex than inductively coupled plasma mass spectrometry (ICP-MS).

The development of at-line or on-line monitors for uranium with isotopic analysis capability focuses on the evaluation of two laser techniques, laser-induced fluorescence (LIF) and cavity ringdown spectroscopy (CRDS), in combination with an inductively coupled plasma (ICP). The ICP serves as a sample atomization source, providing free uranium atoms and ions for LIF and CRDS measurements. For LIF, typical limits of detection (LODs) are on the order of parts-per-million (ppm) to parts-per-trillion (ppt), depending on the oscillator strength of the transition.[1] Thus, LIF has the required sensitivity to detect radionuclides at low concentrations. High-resolution laser spectroscopy permits isotopic species to be differentiated from other isotopes of the same element. Because of the mass difference, the energy levels (and hence the absorption/emission wavelengths) of different isotopes are slightly shifted from one another. Combined with an optimized ICP source, LIF will address a DOE need for a rapid determination of concentrations and isotopic abundances of long-lived radionuclides in order to assure process control and product acceptance.

CRDS is a relatively new spectroscopic technique based on measurement of the decay time for laser light trapped in a stable optical cavity.[2] The presence of an absorbing species (such as uranium) in the cavity will reduce this decay time by absorbing some of the light propagating in the cavity. CRDS efforts toward isotopic uranium monitoring focus on the construction of a small CRDS unit using diode lasers. These small lasers are available for some wavelengths in the blue region of the spectrum and most wavelengths in the red to near-infrared spectral region. They also possess an extremely narrow linewidth easily capable of isotopic resolution. Our previous CRDS

efforts using a narrow-linewidth pulsed dye laser have demonstrated isotopic resolution of mercury in an ICP, quantifying isotopic abundance features separated by as little as 1.1 ppm.[3] These results suggest that a small, sensitive, and isotopically selective CRDS monitor is feasible. Our typical CRDS solution detection limits achieved thus far range from approximately 1 part-per-billion (ppb) for lead to 20 ppb for mercury.[3,4]

One need currently identified by DOE is the analysis of alpha emitters (U, Pu, Am, etc.) in waste water effluents in the 10-n Ci/mL range. This is typically done with either ICP-MS or alpha scintillation counting (ASC). An ICP-MS can cost several hundred thousand dollars and cannot distinguish between isotopes with similar masses (e.g., Pu-238 and U-238). ASC may require long counting times in order to detect isotopes with low disintegration energies. Reaching detection limits of the caliber of ICP-MS on a low-cost instrument (50,000 to 75,000 dollars) could be greatly facilitated using efficient concentration mechanisms. Currently, materials are available that can extract uranium and other actinides from water matrices. After extraction, actinides are eluted from the concentration media via concentrated acids (ranging from a couple of weight percent to 3 M). The concentration media are typically in the form of coated particles that are mixed with a volume of sample (1 - 2 L) and filtered prior to eluting with acid. These concentration methods are not particularly user friendly. The 3M Company has developed concentration disks for the extraction of transition metals and radioactive Cs, Sr and Tc. They are currently working on extraction disks for actinides. By using extraction disks, a volume of sample can be passed through the disk similar to filtration. Although this eliminates one step from the coated particle concentration scenario, the ultimate concentration method would simply contact the sample with an extraction “tool” that would double as an injection device similar to solid phase micro-extraction (SPME) on GC/MS. These preconcentration methods will be evaluated using LIF or CRDS techniques as well.

Work Accomplished

Cavity Ringdown Spectroscopy

Isotopic resolution of three different uranium transitions was obtained using CRDS. The 286.6, 358.4 and 409-nm transitions have been isotopically resolved, yielding detection limits of approximately 140, 300 and 230 ppb, respectively, for U-235. The U-238 detection limit is slightly higher (600 ppb) for the 286.6-nm line because of a small background absorption line in the plasma. Detection of U-235 at its natural abundance level (0.7%) was demonstrated as well using a U-235 concentration of 1.25 ppm. The ultimate detection limit for U-235 in a natural abundance background has not yet been established. Figure 1 shows both the U-235 (left) and U-238 (right) absorption features obtained in a 1:1 mixture at 2.5 ppm.

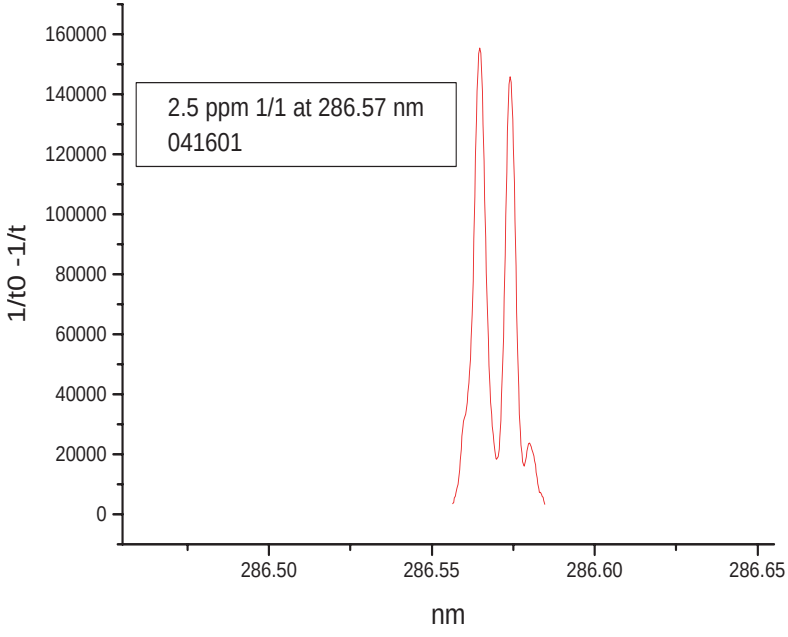

FIGURE 1. Isotope shift at 286.57-nm line, U-235/U-238 = 1/1, 2.5 ppm.

Experiments also were initiated using CRDS to evaluate the isotopic resolution and detection sensitivity of the uranium 424-nm absorption line. However, the substrate of one of the cavity mirrors that had been purchased for this purpose was defective. Two replacement mirrors also suffered from this same defect, indicating that the mirror supplier had purchased a defective set of substrates prior to coating. It will likely take four to six weeks to receive a new set of mirrors for this wavelength. In the interim, a laser ablation sample introduction system on loan from CETAC has been under evaluation using emission measurements from the CRDS group's ICP. Uranium emission has been easily observed in the ICP using a 0.8-ppm NIST solid standard.

Laser-induced Fluorescence

During this quarter, the LIF group has focused on searching for the ideal excitation/detection transition pair for uranium. The ideal excitation/detection combines a large isotopic separation with high transition probability and high lower-state population. In collaboration with the CRDS group, LIF experiments were performed with solutions containing varying amounts of U-235 and U-238 to ascertain if a dye laser (such as CRDS's) is capable of isotopically resolving selected uranium transitions. A number of excitation/fluorescence transition pairs for LIF were investigated using the pulsed dye laser system of the CRDS group. For the 286.6/288.9-nm pair, isotopically resolved LIF excitation spectra yield a detection limit of approximately 150 ppb for both U-235 and U-238. Figure 2 shows the LIF excitation spectra of different concentrations of 1:1 U-235/U-238 solution and demonstrates that isotopic resolution of selected uranium transitions is possible with such a dye laser system. This completes one of the milestones of the LIF portion of this effort. The other two pairs studied, with excitation/fluorescence transitions at 573.4/393.2-nm and 409.0/385.9-nm, respectively, are found to have either low detection sensitivity or small isotopic separation.

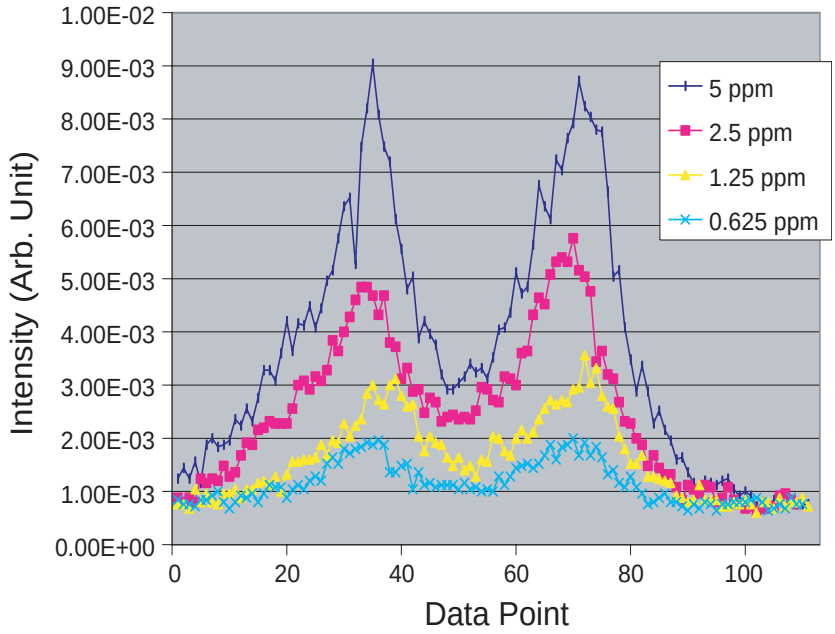

FIGURE 2. Laser-induced fluorescence (LIF) excitation spectra of 286.6 nm, the spectral region for 1:1 mixtures of U-235 and U-238.

Analytical Method Development

Large-volume injection methods have been evaluated using transition metals. Oxalic acid was used as the mobile phase with a 2.0-mL injection loop. No pre-concentration scenarios were used prior to injection. A post column reagent, 4-(2-pyridylazo) resorcinol monosodium salt (obtained from DIONEX), was used to convert the transition metals to an optically active species. The reagent was dissolved in a solution of 1.0-M 2-dimethylaminoethanol, 0.5-M ammonium hydroxide, and 0.3-M sodium bicarbonate (obtained from DIONEX). Detection limits achieved with large volume injections were 10 ppb. Figure 3 is a chromatogram of 10 ppb of Cu and Ni using a 2-mL injection. The peaks for Cu and Ni are well defined and repeatable. Figure 4 shows a chromatogram of 100-ppb sample of Cu and Ni.

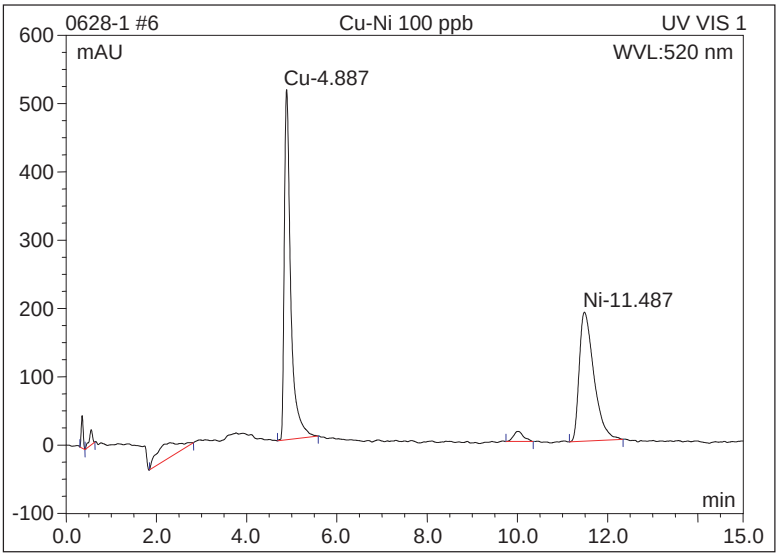

FIGURE 3. 10-ppb concentration of copper and nickel with 2-mL injection.

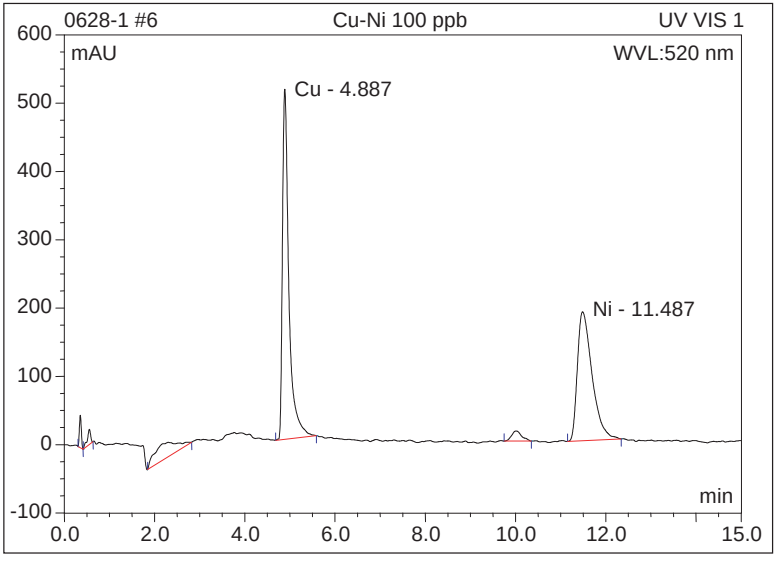

FIGURE 4. 100-ppb concentration of copper and nickel with 2-mL injection.

Work Planned

Cavity Ringdown Spectroscopy

Future CRDS work will focus on evaluating performance for absorption lines accessible to small diode laser systems. This work will initially be carried out using the existing pulsed dye laser prior to the purchase of new diode lasers. If successful, a diode laser will dramatically decrease the size, cost, and complexity of the system. Such a laser can also be tested for use with LIF.

Laser-induced Fluorescence

During the next reporting period, we will focus on upgrading our apparatus for higher spectral resolution and a lower detection limit through the purchase of a dye laser system similar to CRDS's and to an improved detection system. A dye laser with higher resolution will enable us to better resolve the isotopic separation so that we can detect U-235 in the presence of a high concentration of U-238. Our current apparatus is not able to detect U-235 at its natural abundance level (0.7%) because the U-235 LIF signal is overwhelmed by the U-238 LIF signal when 0.625 ppm of U-235 is mixed with 80 ppm of U-238. Our efforts to identify the ideal excitation/detection pair for uranium will also continue.

Analytical Method Development

Future AMD work will demonstrate chelation chromatography techniques, which would allow the analysis of complex samples by removing high concentrations of alkali and alkaline earth metals from the sample. This can be coupled with large volume injections allowing similar detection limits (10 ppb). Also, after successful demonstration of transition metal analysis, AMD will focus on the analysis of rare earth metals using large-volume injections and chelation chromatography.

References

1. X. Hou, S.J.J. Tsai, J.X. Zhou, K.X. Yang, R.F. Lonardo, and R.G. Michel 1997. Laser-excited atomic fluorescence spectrometry: principles, instrumentation, and applications. *Lasers in Analytical Atomic Spectroscopy,* J. Sneddon, T.L. Thiem and Y.I. Lee, eds. New York: VCH Publishers, pp. 83-123.

2. J.J. Scherer, J.B. Paul, A. O'Keefe, and R.J. Saykally1997. Cavity ringdown laser absorption spectroscopy: history, development, and application to pulsed molecular beams. *Chemical Reviews* 97:1:25-51.

3. G.P. Miller and C.B. Winstead. 2000. Cavity ringdown laser absorption spectroscopy. *Encyclopedia of Analytical Chemistry,* R.A. Meyers, ed. Chichester, England: John Wiley and Sons, Ltd., pp. 10734-10750.

4. C. Wang, F.J. Mazzotti, G.P. Miller, and C.B. Winstead. ICP-CRDS: cavity ringdown spectroscopy as a plasma diagnostic. Submitted to *Applied Spectroscopy.*

5. F.J. Mazzotti, C. Wang, S. Tao, J. Mierzwa, C.B. Winstead, and G.P. Miller. Cavity ringdown spectroscopy for analytical mercury measurements. In preparation for submission to *Analytical Chemistry.*

Laser Probe for Technetium Monitor

V. N. Rai, F. Y. Yueh and J. P. Singh

Introduction

Technetium is a product of the nuclear power cycle. The most stable Tc isotope is ^{99}Tc. It has a half-life of 2.1 x 10^5 years and decays via ß-emission. Due to the long half-life and the relatively high yield from uranium decay, DOE desires to separate technetium from non-radioactive and short-life components of the tank waste. They plan to isolate it with other long-life radionuclides in a geologically stable

waste form for safe long-term storage. An on-line monitor for technetium is needed for this waste processing. On-line monitoring during the waste processing will ensure that Tc is properly removed from the processed effluent. The on-line Tc monitor should be able to measure Tc below the 100-µg/L level. The technique should achieve at least a 10% confidence interval at 1000 µg/L.

This technical task focuses on the development and application of laser-induced breakdown spectroscopy (LIBS) to monitor Tc in effluent of Tc processing waste facility. LIBS is a laser-based, non-intrusive, and sensitive optical diagnostic technique for measuring the concentration of various atomic and molecular species in test media.[6,7] It uses a high-power laser beam to produce a laser-induced plasma at the test point. The plasma atomizes and electronically excites the various atomic species present in the test volume in a single step. The intensities of the atomic emission lines observed in the LIBS spectrum are used to infer the concentration of the atomic species. LIBS has successfully demonstrated its real-time monitoring capability in various field tests.[8-15] We will evaluate various techniques which can improve LIBS' sensitivity for Tc measurements.

Work Performed

LIBS spectra of liquid were recorded with a liquid jet system to study the magnetic-field-confined laser-induced plasma. A Q-switched, frequency-doubled Nd:YAG laser (Continuum Surelite III) that delivers energy of ~ 400 mJ in a 5-ns time duration was used to produce the laser-induced plasma. The laser was operated at 10 Hz during this experiment and was focused on the target (liquid jet) using an ultraviolet (UV) grade quartz lens of 20-cm focal length. The same focusing lens was used to collect the optical emission from the laser-induced spark. Two rare earth (neodymium and samarium cobalt) permanent magnets of size 0.5 x 0.5 x 0.125 inches with the pole strength 1.22 T were used for generating the steady magnetic field during this experiment. Both the magnets were fitted in a mild

steel (MS) structural arrangement separated by ~ 5 mm, which provided an ~ 6-KG magnetic field. The magnet system was held in such a way that the liquid jet passed vertically between, and at an equal distance from, the two poles. The laser was focused on the jet through two MS bars such that the plasma plume expanded in a nearly uniform magnetic field.

LIBS spectra of various elements (Mn, Mg, Cr, Ti and Fe) present in the form of aqueous solution were recorded in the absence and presence of the steady magnetic field of ~ 6 KG. These spectra were analyzed to better understand the behavior of atomic or ionic emission from the plasma plume with a change in the laser and plasma parameters. It was found that the intensity of the line emission from the plasma plume shows an increase in the presence of magnetic fields. This increase was found consistent irrespective of whether the line emission is from neutral atoms or from the ions. The increase in the emission signal ranges from 1.5 - 3 times and varies from element to element.

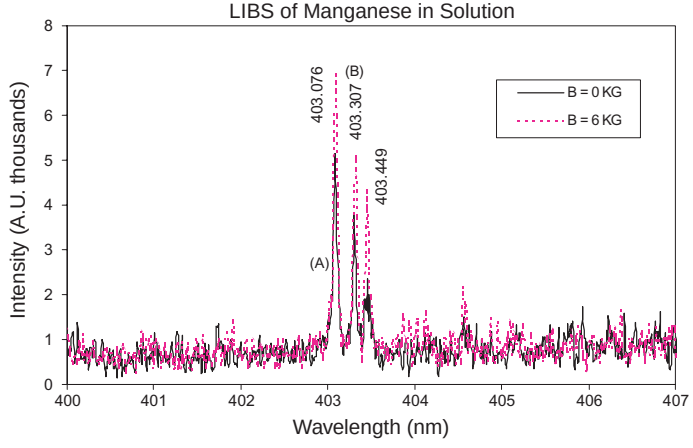

FIGURE 5. LIBS spectra of Mn recorded without (A) and with (B) the magnetic fields.

Figure 5 shows the LIBS spectra of manganese in the absence and presence of magnetic fields. The background emission from the plasma decreases in the presence of magnetic fields. The line emission intensity shows either saturation or decrease towards a higher laser energy side. The threshold for saturation depends on emission property of the element as well as on the laser energy and magnetic field.

Table 1 shows the enhancement factor in the emission intensity for various elements (Mg, Cr and Ti) for different laser parameters and in the presence of magnetic fields. The increase in the signal in the magnetic field was attributed to an increase in the effective density of plasma in the plume due to magnetic confinement. The temperature of the plasma goes down as the plasma expands after the

TABLE 1. Variation in the enhancement of LIBS intensity at different line emission wavelength for magnesium (Mg), titanium (Ti) and chromium (Cr) in solution when excited at two different laser energy.

	Emission Wavelength (nm)	Enhancement Factor (G)	
		Laser Pulse Energy	
		140 mJ	280 mJ
Mg (10 ppm)	279.55	1.71	1.14
	280.27	1.66	1.25
	285.29	1.56	1.49
Ti (100 ppm)	363.55	1.26	1.52
	364.27	1.14	1.42
	365.35	1.29	1.4
Cr (10 ppm)	425.44	1.56	1.81
	427.48	1.5	1.82
	428.97	1.55	1.99

laser pulse. The combined effects of higher plasma density and lower plasma temperature result in an increase in the rate of three body

recombination of the plasma particles, which ultimately results in an increase in the plasma emission. These observations were explained on the basis of the model which indicates that enhancement is mainly correlated with the decrease in the plasma expansion velocity in magnetic fields and is mainly dependent on plasma beta value, which is the ratio of plasma kinetic energy to magnetic energy. It shows that as the plasma beta goes down, emission intensity increases. It further indicates that the enhancement factor can be increased to an even higher value by keeping the plasma beta value close to one by increasing the magnetic field.

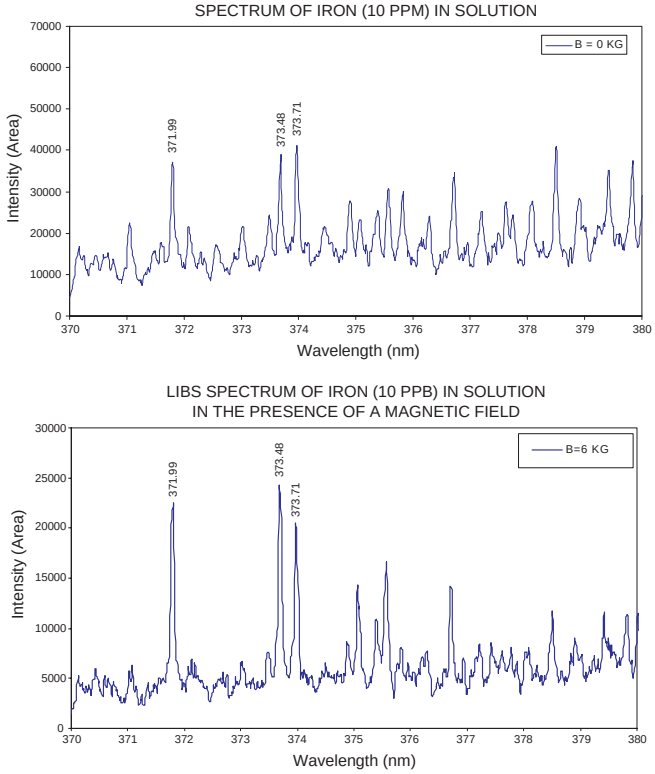

FIGURE 6. LIBS spectra of Fe recorded without (top) and with (bottom) the magnetic field.

Figure 6 shows the LIBS spectra of iron (10 ppb) in the absence and the presence of a magnetic field. The main effect of magnetic fields on the iron spectra was the suppression of the background emission to nearly one third of its original value, which makes the line emission prominent and ultimately increases the S/B ratio. An enhancement of ~ 2.5 times was noted in the S/B ratio for iron emission at the laser energy of ~ 280 mJ. This indicates that with the help of the external magnetic field it is possible to detect iron concentration of even less than 10 ppb.

Work Planned

The results of the preliminary experiment with the magnetic field indicate that the sensitivity of the LIBS system for the liquid sample can be increased by nearly two times using the external magnetic field of ~ 6 KG. The combination of an external magnetic field with other signal-enhancing techniques, such as using purge gas around the liquid jet and the two pulse excitation technique, may be useful in enhancing the sensitivity of the system by an order of magnitude. Work to study the possible enhancement from these techniques will continue.

References

6. D.A. Cremers and L.J. Radziemski. 1987. Laser plasmas for chemical analysis. *Laser Spectroscopy and Its Application*, L.J. Radziemski, R.W. Solarz, J.A. Paisner, eds. New York, Marcel Dekker. Ch. 5, p. 351.

7. L.J. Radziemski and D.A. Cremers. 1989. Spectrochemical analysis using plasma excitation. *Laser Induced Plasmas and Applications*, L.J. Radziemski and D.A. Cremers, eds. New York, Marcel Dekker. Ch. 7, p. 295.

8. J.P. Singh, F.Y. Yueh, H. Zhang. 1997. *Process Control and Quality* 10:247.

9. J.P. Singh, H. Zhang, F.Y. Yueh and K.P. Carney. 1996. *Applied Spectroscopy* 50:764.

10. J.P. Singh, H. Zhang and F.Y. Yueh. February 1996. Transportable vitrification system shakedown test, Westinghouse Savannah River Corporation and Diagnostic Instrumentation and Analysis Laboratory: laser-induced breakdown spectroscopy measurements. US DOE Contract No. DE-FG02-93CH-10575. DIAL 10575 Trip Report 96-1.3.

11. J.P. Singh, H. Zhang and F.Y. Yueh. April 1996. DOE and EPA continuous emission monitoring test at EPA National Risk Management Research Laboratory (NRMRL). US DOE Contract No. DE-FG02-93CH-10575. DIAL 10575 Trip Report 96-2.

12. J.P. Singh, H. Zhang and F.Y. Yueh. 1996. Plasma arc centrifugal treatment PACT-6 slip stream test bed (SSTB) 100-hour duration controlled emission demonstration (CED) test. DIAL Trip Report 96-3.

13. J.P. Singh, H. Zhang and F.Y. Yueh. September 1997. DOE and EPA continuous emission monitoring test at EPA National Risk Management Research Laboratory (NRMRL). DIAL Trip Report 97-1.

14. H. Zhang, F.Y. Yueh and J.P. Singh. 1999. *Applied Optics* 38:1459-1466.

15. H. Zhang, F.Y. Yueh and J.P. Singh. 2001. *Journal of Air & Waste Management Association* 51:174-180.

TASK 2

Development of Tools for Long-term Monitoring

Monitoring Plant Physiological Status in Contaminated Environments by High-resolution Spectral Imaging

Yi Su and David Monts

Introduction

Purpose

The goal of this project is to use remotely sensed data to monitor the physiological status of plants growing on contaminated DOE sites. The physiological status will be used as an indicator of the presence of pollutants, such as heavy metals or radioactive species, in the growing environment. This capability will enhance DOE's capability for cost-effective long-term monitoring of contaminated sites.

Plant reflectance is governed by leaf surface properties and internal structure, as well as by the concentration and distribution of biochemical components, and thus remote analysis of reflected light can be used to assess both the biomass and the physiological status of a plant. Particular spectral bands and band combinations (often referred to as reflectance indices) for monitoring crop stress resulting from nitrogen deficiency, water deficiency, etc., have been reported using

remote sensing. We propose to monitor the impact of contamination, such as by heavy metals, on plant physiological status. A computerized spectral imaging system will be applied to take images of plants growing in a controlled environment with known concentrations of heavy metal contamination. Spatial and temporally distributed information extracted from images of different spectral bands will be part of this plant physiology study. The focus of this project is to search for indices (signatures) that indicate the impact and the content of heavy metals in the leaves and canopies of live plants. This ground-level study will also help to determine whether the physiological reflectance signals are stronger than disturbances introduced by factors such as the position of the sun, heterogeneity of the landscape, or atmospheric interference. The resulting information will be essential to determine whether remote sensing technology can be used for long-term monitoring of the spread of pollutants at some of the DOE closed sites.

Methodology

A portable spectroradiometer system and a spectral imaging system will be applied to monitor plant physiological status in contaminated environments. The spectroradiometer will be used to record reflectance spectra from the plant throughout the growing process. The spectral analysis will provide data on the impact of the contamination on the plant physiology, and also will help determine the key spectral band(s) (signature) related to specific contamination. A spectral imaging system, which is based on the outcome of Task 3.2 (On-Line Multispectral Imaging of Thermal Treatment Process) of last year's Cooperative Agreement, will provide the spatial analysis. The spectral imaging system will help us overcome problems related to mixtures in the field of view, such as soil, dry leaves, stems, and shadows. The information extracted from spectral images will also be used to study plant canopy structure change during the growing process.

This is a multi-year project. The first year will be devoted to a laboratory study: a laboratory-size plant bed will be used to study the impact of selected metal species on plant physiology status. The second and third years will be devoted to studying plants grown under a controlled natural environment for conditions similar to those that pertain to selected DOE sites; the plants affected by contamination will be studied in a potted-plant growing facility in a natural environment. The following years will be devoted to DOE site-specific studies.

Work Accomplished

During this reporting period, we have recruited a graduate student with expertise in agriculture and remote sensing to work on this project. At Mississippi State University, researchers from the Department of Plant and Soil Science and the U.S. Department of Agriculture operate a state-of-the-art facility for growing a variety of agricultural crops under tightly controlled conditions that enable the exact amount of nutrients that the crops receive to be precisely controlled. We have formulated a detailed experimental plan after an extensive literature survey and after consulting with MSU plant scientists. Two plant species (*brassica juncea* and barley) have been chosen for our initial study of heavy metal accumulation and monitoring. *Brassica juncea* is well documented as an accumulator of cadmium and zinc. Barley was chosen as an example of grasses. Moreover, the number of plants necessary for statistical significance and the number of plants per pot were determined. A dedicated portable spectroradiometer system (ordered and received during this quarter) will be used to monitor the physiological status when the plants are exposed to selected amounts of heavy metals. A mobile plant cart has been designed and constructed; this cart will allow the plants to be grown under identical environmental conditions while allowing different plants to be subjected to differing amounts of heavy metals without cross-contamination of the plants. Necessary chemicals, such

as nutrients and cadmium and zinc compounds, have also been ordered in accordance with the experimental plan.

At a DOE Long Term Monitoring Workshop in Orlando in June, we met researchers from the Savannah River Site who are interested in collaborating with us on this project in order to ultimately apply this technique to their site. This collaboration is being pursued.

Work Planned

We will begin planting plants and monitoring the physiological status of plants subjected to different heavy metal contamination as soon as the chemicals and nutrients ordered arrive. The spectroradiometer will be used to record reflectance spectra from the plants throughout the growing process.

Moisture Fiber-optic Diode Laser Sensor

R. Jindal, S. Tao and J. P. Singh

Introduction

Moisture fiber optic sensors can be used for monitoring humidity in harsh environments, such as factories with electromagnetic noise unacceptable for regular capacitance-based moisture gages, radioactive waste storage facilities, etc. Several U.S. DOE waste tank storage sites, such as the Hanford site, lack the ability to monitor water in subsurface rear storage. The main purpose of this study is to prove the concept of the sensor, make preliminary samples, and experimentally find a way to improve their performance. The sensor is proposed to be realized using two methods: 1) using a swell-able hydrogel to produce micro-bending in fiber[16], and 2) using an approach based on the absorption of the evanescent tail of the light propagating in fiber[17,18].

Both approaches would be tried and tested for various levels of moisture detection.

Work Accomplished

In the first part, we obtained a good hydrogel composition, which needed to be fully reversible. This experiment yielded a fully reversible fiber-optic humidity sensor, but the total reaction time was found to be in hours (Fig. 7). We then decided to use the evanescent wave absorption phenomenon by coating an appropriate chemical on the fiber core. Our initial challenge was to find an effective way to remove the fiber cladding, as the interaction with the evanescent wave can only be made very near to the fiber core. At first, acetone was used, as mentioned by the fiber manufacturing company. But later on we found that it was not a fully effective method; burning off the cladding proved to be more effective. We also designed a small glass chamber with an inlet and an outlet for passing the dry and wet gases to obtain a moisture variation in the chamber. The cladding was removed from 200-µm fibers. The exposed portion of the fiber was subsequently coated by an aqueous solution of 2% PVA and 1% $CoCl_2$. The fiber was then placed in the environment chamber. The experimental setup is shown in Figure 8. The relative humidity (RH) in the chamber was varied rapidly by passing wet and dry gases alternatively. The fiber probe was found to respond quite well and rapidly during an RH change from 15% to 95%. Encouraged by this, we decided to make a slower change in RH and monitor the change in fiber output at various levels of humidity, calibrating it against a commercially available RH probe. We then found that the fiber probe was actually responding to RH only above 78% and is quite fast in that range of RH (Fig. 9). Fibers of different diameters were also tried, but were found to produce similar results.

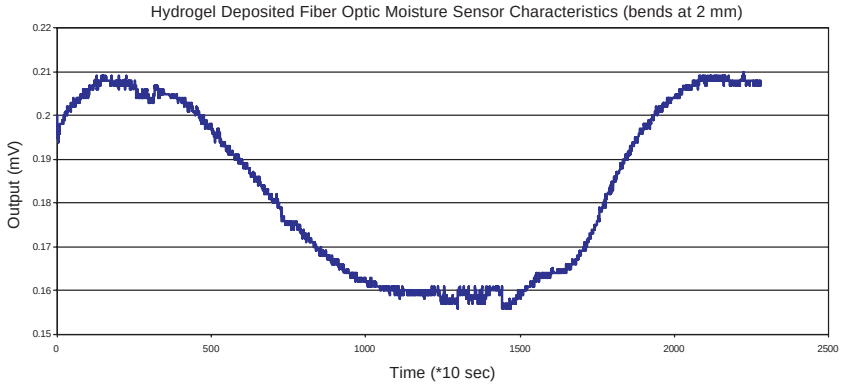

FIGURE 7. Time response of the hydrogel based fiber sensor.

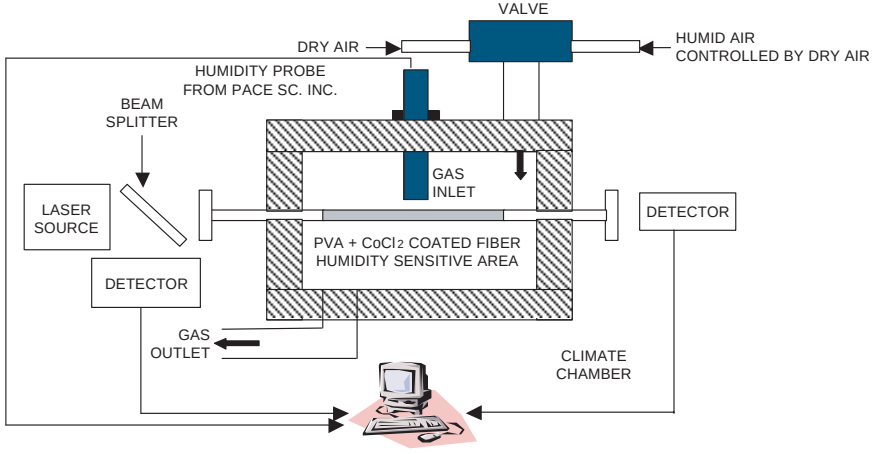

FIGURE 8. Experimental set-up.

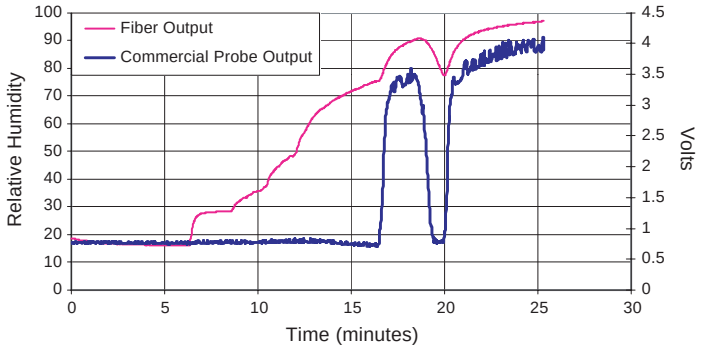

FIGURE 9. Behavior of fiber optic probe versus the standard probe at various humidity levels.

Work Planned

The primary requirement in this period is to find an effective way of enhancing the range of operation of the sensor to lower humidity levels. Once that is achieved, different fibers will then be tested to optimize the behavior of the sensor.

References

16. W.C. Michie, et al. 1995. Distributed sensor for water and pH measurements using fiber optics and swellable polymeric systems. *Optics Letters* 20:103-105.

17. A.P. Russell and K.S. Fletcher. 1985. Optical sensor for determination of moisture. *Analytica Chimia* 170:209-216.

18. R. Hypszer and H.J. Wierzba. 1997. Fiber optic technique for relative humidity sensing. *SPIE Proceedings* 3054:145-150.

Application of Imaging Techniques

Introduction

Purpose

Imaging techniques can be utilized to provide solutions to a wide variety of issues facing DOE, ranging from process control to off-line melter inspection to long-term monitoring. This effort will develop the techniques and instrumentation needed to address these needs.

Spectral images are obtained by positioning a narrow-bandwidth bandpass filter in front of a camera. The bandpass spectral region of the filter is selected to coincide with the emission of an atomic or molecular species of interest or to coincide with regions of the spectrum containing only blackbody emission. With proper selection of wavelengths, information about the spatial distribution of species present or about temperature distribution can be derived from these images. Spectral and thermal imaging can provide DOE with information crucial to its decision-making processes.

There is a commonality to the data collection hardware, data and analysis software, and the data-sifting techniques necessary for applying imaging techniques. This effort expands on existing expertise to develop imaging collection and analysis systems that address a wide variety of DOE's needs. Our efforts this grant year concentrate on (but will not be limited to) inspection of off-line Joule-heated melters to determine where and how much exceptional wear occurred, and also to determine the location, size, and composition of the deposited materials.

Methodology

Our efforts will concentrate on DOE's needs for inspection of off-line Joule-heated melters to determine wear patterns and the location and composition of deposits; this information will aid in the design of the next generation of HLW melters. Narrow bandpass filters will be combined with block cameras to enable spectral imaging within the melter. DIAL's imaging capability will be extended to the near-infrared spectral region. Diffuse reflectance spectroscopy will permit selection of proper observation wavelengths. Means of quantitatively determining the extent of wear or amount of deposition will also be developed based on two techniques: Fourier transform profilometry (FTP) and stereo vision. DIAL has previously demonstrated that its FTP system can quantitatively determine the volume and depth of removed material to high accuracy. Improvements will include: (1) improvement of the fringe pattern projection system, and (2) improvement of the phase unwrapping algorithm; this upgrade will resolve the 2 π-phase discontinuity associated with abrupt changes in surface height. A second imaging technique, stereo vision, will also be developed as a means of determining the depths and heights of surface features. Stereo vision provides determinations of depths and heights by combining images simultaneously recorded by two cameras. Knowledge gained from and techniques developed for characterization of off-line melters can also be applied to characterization of on-line melters. A collaborative arrangement has been established with SRS's DWPF facility to inspect their melter at an appropriate time. Efforts are underway to establish a similar relationship with West Valley.

Techniques have been developed to detect hot spots, thermal distribution, characterization of vegetation, detection of uneven surfaces, etc., from imaging data. This year's effort also aims at enhancing the techniques already developed here and to develop new techniques and capabilities utilizing statistical as well as intelligent system approaches. While statistical methods provide linear relationships,

artificial neural networks are apt to deal with non-linear relationships inherent in the data. Besides these, rule-based techniques would derive heuristic relationships. The existing capabilities will be extended to characterize soil, melters, and vegetation from uni- and multi-spectral images. This will enable long-term monitoring to detect the presence and variation of trace elements, especially hazardous ones in plants. The ability to classify regions of interesting characteristics will provide valuable information regarding contamination in soil and other media. One of the objectives of this effort is to go beyond typical data analysis methods in pursuit of discovering new relationships, thereby sifting information hidden in the data.

Work Accomplished

Profilometry

Development of the Fourier transform profilometry (FTP) system continued. The phase shift extraction process has been improved by replacing a one-dimensional fast Fourier transform (1D-FFT) that was used on a line of pixels within an acquired image (as in Fig. 10), with subsequent line-by-line processing to construct the phase shift map for the whole image. The phase shift extraction analysis software has been modified by substituting a 2D-FFT module in place of the 1D-FFT.

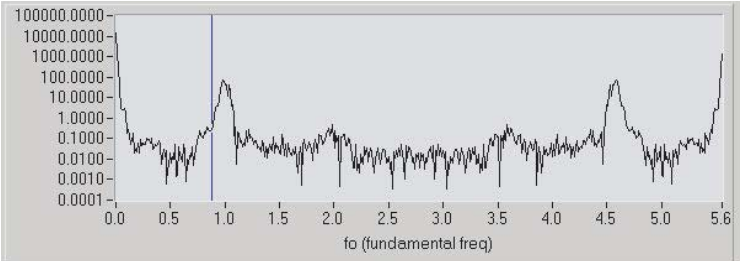

FIGURE 10. Result of 1D-FFT from a line of pixel intensity within the image acquired.

As shown in Figure 11, the fundamental frequency in both X and Y directions were selected for phase extraction, and the corresponding region of interest (ROI) is highlighted on the FFT image, as in Figure 12.

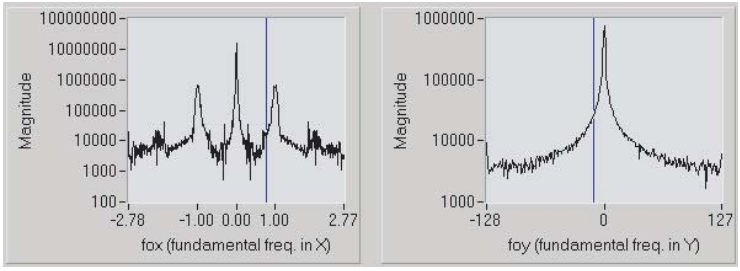

FIGURE 11. Both X and Y directions are considered in frequency range selection for the phase extraction.

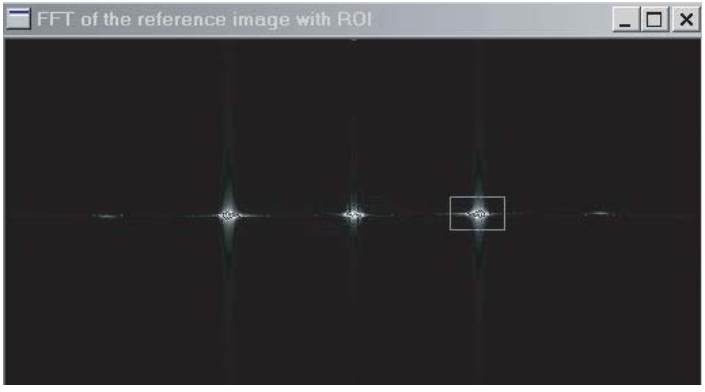

FIGURE 12. Selected ROI in 2D-FFT image.

With the additional Y-direction consideration enabled by adopting 2D-FFT, the result of the final surface profile has been improved. As shown in the Figures 13 and 14, there are much smaller residuals (discontinuity pairs) in the phase shift map from 2D-FFT than the map from 1D-FFT.

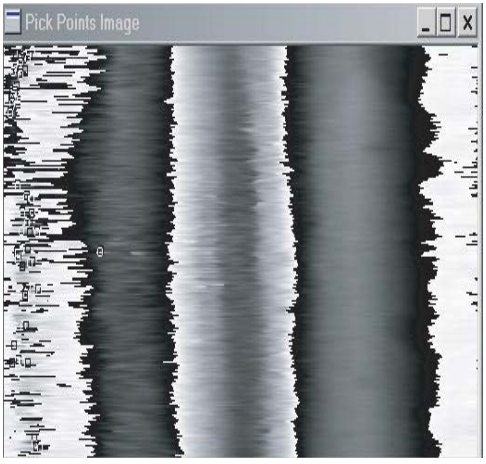

FIGURE 13. Residual map generated by 1D-FFT.

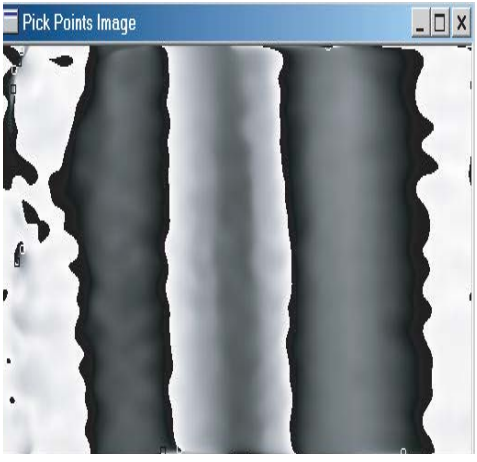

FIGURE 14. Residual map generated by 2D-FFT.

The improvement can be realized in the final target sand pile 3D-views as in Figures 15 and 16.

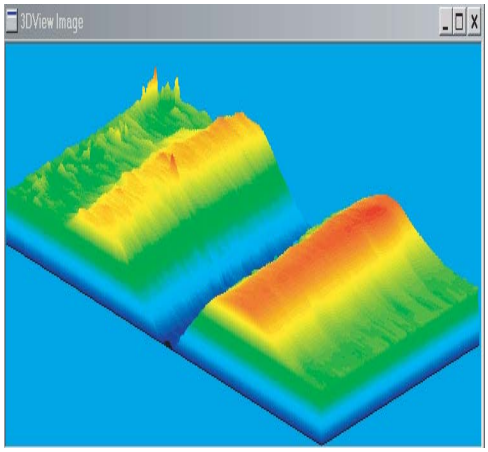

FIGURE 15. 3D view result of sand pile measurement using 1D-FFT.

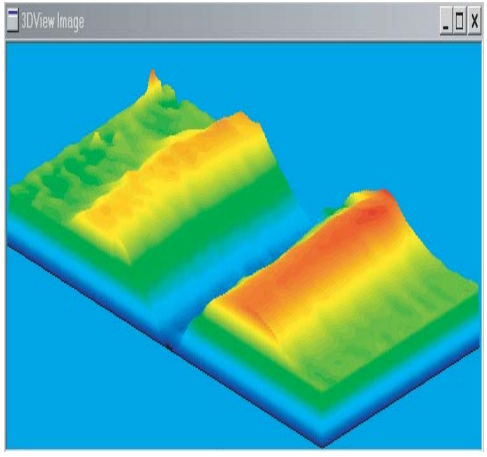

FIGURE 16. 3D view result of sand pile measurement using 2D-FFT.

Also for the final surface profile, a user-predefined median filter has been integrated into the analysis system to smooth the height

spikes, which generally result from errors introduced in data acquisition and from the preceding analysis phases.

Thermal Imaging

In an effort to expand thermal imaging's spectral response region, a near-infrared (NIR) camera system has been obtained. Characterization of the NIR camera's baseline parameters has begun. The correction mask for the bad pixels exist in the InGaAs focal plane array of the NIR camera, as shown in the Figure 17.

FIGURE 17. Established bad pixels (as shown in white dots) mask.

Using the on-line bad pixels correction module, which uses a non-linear image median filter to modify the acquired raw image, raw and corrected images can be obtained in near-real time, as shown in Figures 18 and 19.

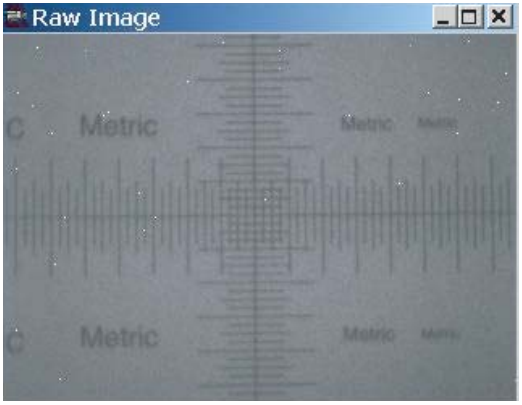

FIGURE 18. Acquired raw (uncorrected) image.

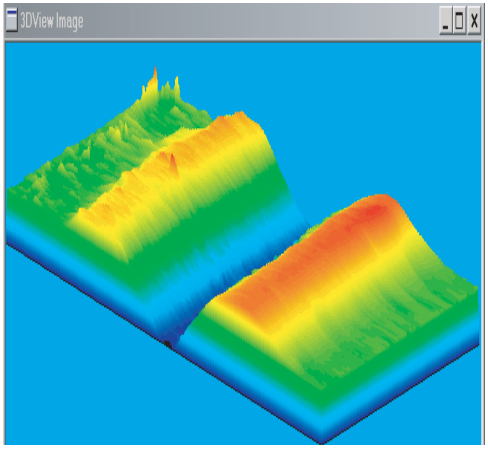

FIGURE 19. On-line median filter corrected image.

The FPA's dark current pixel intensity map has also been acquired for the future calibration reference, as has its intensity histogram (Fig. 20).

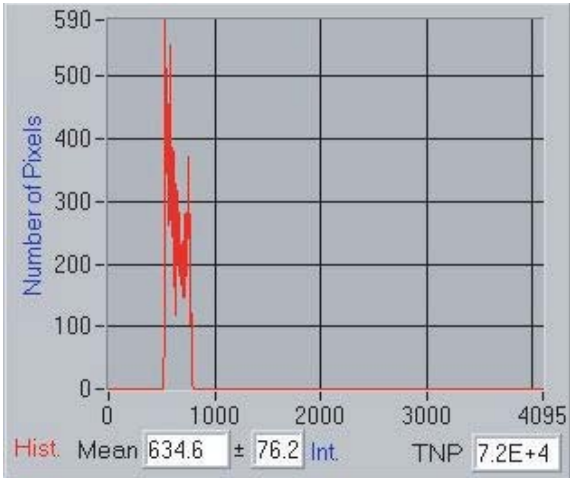

FIGURE 20. Histogram of FPA's dark current intensity.

A study of the image file format [Portable Network Graphics (PNG)] was initiated. The PNG file format is used for loss less compression of images acquired from DIAL's non-8-bit monochrome cameras.

In support of the RIC-AVS project, the thermal imaging systems were used to monitor a batch-melting process. The melt surface temperature map is provided to the system operator in near-real time.[19] A new version of the imaging system drivers has been installed. Modification of current system packages has been completed for the thermal imaging system.

Spectral Imaging

Significant progress has been made toward the development of a computerized spectral imaging system. This system consists of a five-filter filter wheel and a CCD camera; the position of the filter wheel, the number and duration of spectral images, and the time delay between spectral images are all under computer control. The system

has been tested in our laboratory for real-time spectral image acquisition. This development effort included integration of image collection and analysis into a single computer program. The system has been tested by recording 307-nm spectral images of OH emission in an ICP plasma. Additional modifications enable the software to properly synchronize data acquisition of spectral images with our pulsed laser: we can now capture spectral images produced by every laser shot. Previously, the synchronization was not well done and spectral images of many laser shots were missed.

The UV AOTF manufacturer is making progress toward completion of our system; delivery is currently expected in mid-summer.

Information Sifting

The information-sifting effort has concentrated on locating spectral and image libraries that will aid in the analysis of spectral images as well as diffuse reflectance spectra. The images and data will be generated as part of the off-line melter inspection effort and the plant monitoring effort. Development of a search engine for use with these libraries has begun.

Work Planned

Profilometry

Work will continue on the study of the phase unwrapping algorithms[20,21] for target areas that have large height discontinuities and/or surface isolations. Efforts to integrate a higher-resolution digital camera in order to increase the target sampling frequency will continue. Modification of the current system packages for the new set of system drivers will continue.

Thermal Imaging

We will continue our efforts to integrate the InGaAs CCD bad pixels correction mask into the on-line imaging pixel correction and the computer-controlled exposure-time settings software modules. Investigation of a new graphical file format (PNG) will continue. Our efforts on thermal calibration and system software modification for the thermal imaging system utilizing a high-resolution visible digital camera will continue.

Spectral Imaging

During the next quarter, the spectral imaging system will be upgraded, as we plan to purchase improved data-acquisition boards. Efforts to integrate data acquisition and data analysis into a single computer program will continue.

Information Sifting

We still continue our effort to examine spectral libraries. Algorithms are needed that can (1) locate a spectral library, (2) select a suitable reference spectrum, and (3) identify the spectrum that most closely matches the reference spectrum. We plan to start developing a prototype for a search engine and for spectral matching. Software tools to develop the system will be acquired.

References

19. AVS-RIC report.

20. D.C. Ghiglia and M.D. Pritt. 1998. *Two-dimensional phase unwrapping.* John Wiley & Sons, Inc.

21. Mitsuo Takeda, et al. 1997. Frequency-multiplex Fourier-transform profilometry: a single shot three-dimensional shape measurement of objects

with large height discontinuities and/or surface isolations. *Applied Optics* 36:22.

Acronyms

1D-FFT	one-dimensional fast Fourier transform
2D-FFT	two-dimensional fast Fourier transform
AOTF	acousto-optical tunable filter
AVS	advanced vitrification system
CCD	charge-coupled device
DWPF	Defense Waste Processing Facility
FPA	focal plane array
FTP	Fourier-transform profilometry
ICP	inductively coupled plasma
InGaAs	indium gallium arsenide
NIR	near infrared
OH	hydroxide radical
PNG	Portable Network Graphics
RIC	Radioactive Isotope Consortium
ROI	region of interest

SRS	Savannah River Site
UV	ultraviolet

TASK 3

Hanford Tank Waste Chemistry

Saltcake Dissolution

R. K. Toghiani, V. A. Phillips, D. Selvaraj, and J. S. Lindner

Introduction

This project is a continuation of the work previously reported on the dissolution of Hanford waste saltcakes. A main portion of the work is to continually validate and upgrade a thermodynamic equilibrium model, the Environmental Simulation Program (ESP) as applied to the Hanford wastes. Toward this end a number of significant accomplishments have been reported previously.[22-26] These include the evaluation of the code for the dissolution of saltcakes varying in composition through a comparison of model predictions with experimental results on core samples performed at the site, the use of the model to aid in the development of remediation strategies for Hanford tank 241-SY-101, an evaluation of data preprocessing, and the experimental determination of the solubility of natrophosphate, a double salt observed in the tank wastes.

A major focus is in bolstering the predictions of the code through comparison with experimental data and with other thermodynamic models such as SOLGASMIX. Accurate data called by the model are

an essential requirement for quantitative code predictions; however, it must be noted that evaluation of the thermodynamic interactions between all of the species existing in the waste streams is not possible. The path, therefore, has been to concentrate on those anions such as nitrate, nitrite, hydroxide, sulfate, phosphate, fluoride, oxalate, carbonate and cations, sodium, aluminum, calcium, nickel, uranium, etc., and the associated solids from these species that comprise the majority of the waste composition. Once assured that the code predictions accurately reflect the thermodynamics of these systems, we can further upgrade the model to include other species of considerably lower concentration. The project is divided into three tasks, as summarized below.

Task 1. Comparison of ESP to other thermodynamic equilibrium codes

The model has been shown to provide agreement with literature data for the solid liquid equilibrium behavior of many of the saltcake constituents at both high and low ionic strengths. Nonetheless, questions will remain on the application of the model to situations in which the ionic strength is high, owing to the extrapolation of fundamental electrolyte theory to regions of high ionic strength. Theoretical calculations for the most prevalent solid in the waste, sodium nitrate, will be performed at high ionic strength and compared to an alternate model developed by M. Ally at ORNL. Comparisons with the SOLGASMIX model, in collaboration with C. F. Weber (ORNL), will be performed for the sodium-fluoride-sulfate system. Companion solubility experiments will be made on this system to improve the ESP database (Task 3).

Task 2. Comparison of ESP predictions to saltcake dissolution experiments

Previous work has characterized saltcakes with roughly four typical compositions, as anticipated in the Hanford tank wastes. These studies have indicated that ESP can be used to predict the dissolution behavior of the majority of the solids present. An exhaustive search for other types of saltcake compositions was conducted recently by

D. L. Herting of Fluor Hanford, resulting in the identification of two additional tanks with different composition distributions. A sample from tank TX-113 will be evaluated this year. In addition, recent interest in pretreatment and retrieval operations has indicated that there may be some concern when supernates from different waste streams are combined. ESP will be used with the predicted supernates from some of the previous saltcake dissolution studies to examine the propensity of solids formation under expected operating conditions. Predictions will be compared with ongoing experimental work at the site.

A conference on the dissolution of saltcakes will be organized, and this forum will provide for extended discussions on the progress and results of the work and on future programmatic directions. Reports on the saltcake dissolution studies and on the outcomes of the saltcake dissolution conference will be provided.

Task 3. Improvements and user documentation for the ESP model

Some deficiencies have been shown to exist within the ESP databanks.[22] Of high interest is the determination of solubility data for double salts. Solubility studies for Na_3FSO_4 will be conducted and compared to the results of the prior literature and the calculations performed in Task 1. Additional studies on the extent of hydration as a function of ionic strength will be performed for Na_2CO_3 and Na_3PO_4.[27] Experiments are also planned for NaF at elevated ionic strength and in the presence of $NaNO_3$.

Considerable effort has been expanded in learning the most appropriate ways in which to develop and run ESP simulations. These will be documented and forwarded to customers at Hanford for incorporation in the *ESP User Manual.*

Work Accomplished

Results and Discussion

Saltcake dissolution studies

In the previous quarterly report, simulations of the FY01 saltcakes at 21°C were presented. In an effort to explain behaviors observed in the comparison of simulation results to experimental measurements taken by Herting, expanded simulations for saltcake BY-109 were completed during this quarter. In Figure 21, it is observed that the fluoride concentrations predicted by ESP at cumulative dilution additions of 100 and 150% by weight are identical.

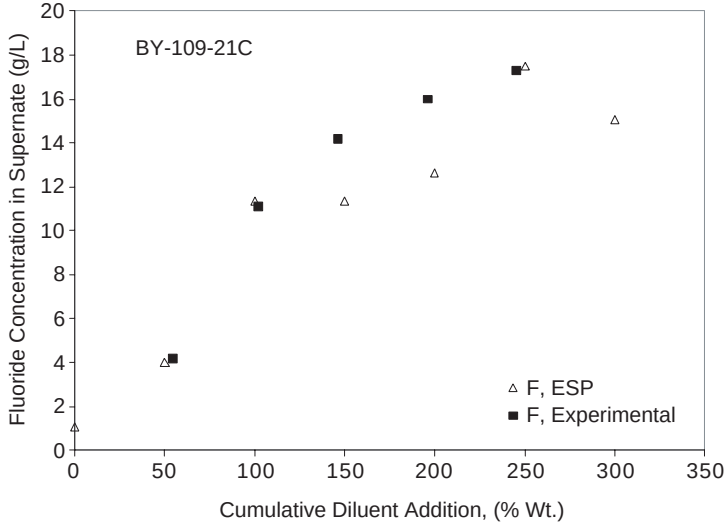

FIGURE 21. Liquid phase concentrations for fluoride anion – Saltcake BY-109.

Similar behavior is observed for the sulfate concentration at these diluent additions, as shown in Figure 22. The fluoride concentration is over-estimated by ESP at the 150% diluent addition level, while the sulfate concentration is under-estimated by ESP at the 100% diluent

addition level. To better understand the simulation results, we performed revised simulations in which the diluent was added in small doses, and equilibration with the added dose was predicted without separation of the bulk phases. This approach gave rise to a series of predicted concentrations for the various anions.

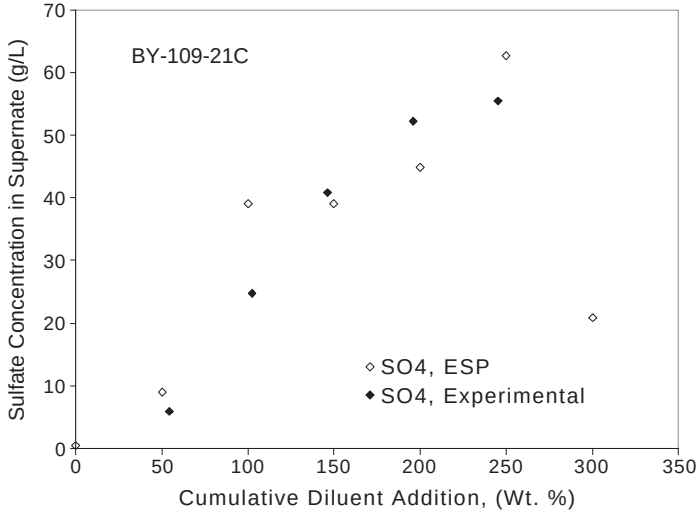

FIGURE 22. Liquid phase concentrations for sulfate anion – Saltcake BY-109.

The predicted concentrations for fluoride are shown along with the experimental data from Herting in Figure 23, while for sulfate, the same comparison is given in Figure 24.

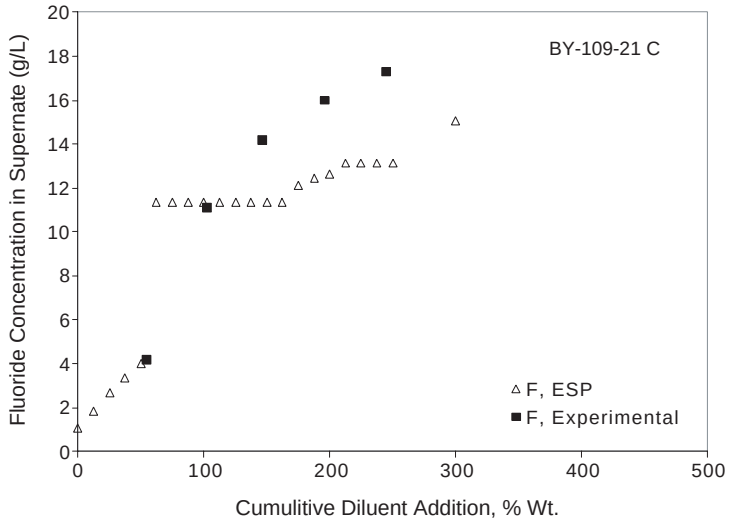

FIGURE 23. Revised liquid phase concentrations for fluoride anion – Saltcake BY-109.

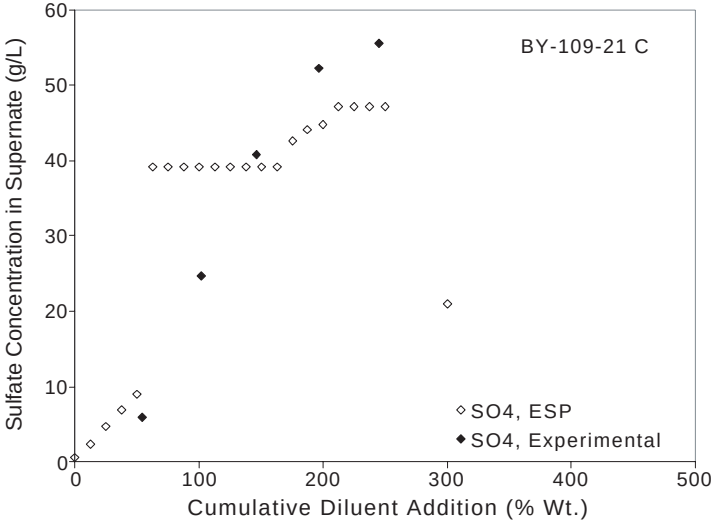

FIGURE 24. Revised liquid phase concentrations for sulfate anion – Saltcake BY-109.

From these comparison plots, it is apparent that the liquid solution in equilibrium with the existing solid phase has an invariant composition regardless of the amount of diluent added in the range of 62.5% to 162.5% cumulative diluent addition. Over this range of diluent additions, ESP predicts that two double salts [Na_3FSO_4, $Na_7F(PO_4)_2 \cdot 19H_2O$] and a single salt (NaF) are present in the solid phase. The plateau in the concentrations of fluoride and sulfate corresponds to an invariant point. In a ternary system, for example, the NaF-Na_2SO_4-H_2O ternary, this behavior would occur when the solid phase (two species) is in equilibrium with the liquid phase. According to Gibb's phase rule, the composition of the liquid phase would be fixed. While this saltcake is certainly more complex compared to a simple ternary system, the behavior observed in the predicted results indicates that the solid phase partitioning between pure sodium fluoride and the sodium-fluoride-sulfate double salt calculated by ESP is in disagreement with the experimental results. Solid phase characterization for the BY-109 saltcake is currently underway at Hanford and results from this characterization will aid in understanding the discrepancies observed between ESP predictions and the experimental concentrations.

Experimental studies of select double salt systems

Solubility studies on the Na-F-SO_4-OH system. Experimental solubility measurements for the sodium-fluoride-sulfate-hydroxide system were completed during the previous quarter. During the current quarter, preliminary examination of theses data using the available regression tools in ESP was undertaken. A multi-step approach was taken in fitting the available experimental data. The data in aqueous solution (at both 25°C and 50°C) where the solid phase was identified as the sodium-fluoride-sulfate double salt was used to adjust the constants in the KFIT expression used by ESP. This expression, given in Eq. 1, is used by ESP to estimate the equilibrium between solid and liquid phases:

$$ln(KFIT) = A + B/T + CT + DT^2 \quad \textbf{(EQ 1)}$$

In the PUBLIC database that accompanies version 6.5 of the ESP program, the *KFIT* expression for the sodium fluoride-sulfate double salt includes only parameter *A*. This is a selection, made by the developers of ESP, based on the temperature range of the available literature data (25 to 35°C). The experimental data obtained in this laboratory effectively double the number of data points as well as extend the temperature range to 50°C. However, the solubility of the sodium sulfate-fluoride double salt in aqueous solution exhibits weak temperature dependence. The *D* parameter is typically only required when data exhibit extreme temperature dependence.

Two regression programs were used. Preliminary regression was carried out using the PROCHEM/ELECTROCHEM component of ESP. The parameters in the *KFIT* expression are obtained through adjustment with the norm of the data set determined for each iteration. The data set was regressed twice, first holding the sodium fluoride input fixed while allowing the sodium sulfate input to be adjusted, then holding the sodium sulfate input fixed, with adjustment of the sodium fluoride. Figures 25 and 26 provide comparisons of the regressed data with the original experimental data. These results are provided for the three-parameter *KFIT* expression (*A,B,C* incorporated).

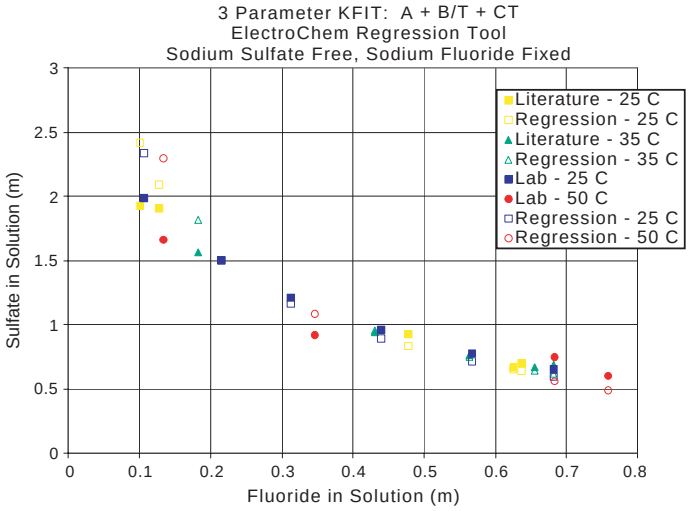

FIGURE 25. Regression results – sodium fluoride sulfate double salt in aqueous solution – sodium sulfate input free; sodium fluoride input fixed.

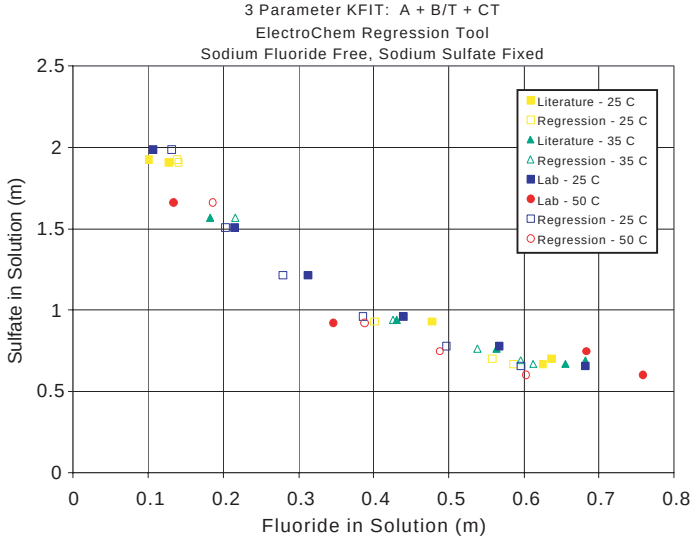

FIGURE 26. Regression results – sodium fluoride sulfate double salt in aqueous solution – sodium fluoride input free; sodium sulfate input fixed.

In Figure 25, it is evident that the adjustments to the sodium sulfate input are larger in the high sulfate region, while in Figure 26, the adjustments to the sodium fluoride input are larger in the high fluoride region. A different approach, using the DOS-based regression tool (REGRESS.EXE) supplied by OLI Systems, Inc., consisted of partitioning the data set into two separate sets that were then regressed simultaneously. The DOS-based regression tool is the newer regression program and allows the incorporation of like-ion interactions. The flexibility of partitioning the data set, so that adjustments are made to sodium sulfate input for high fluoride samples, while made to sodium fluoride input for high sulfate samples, allows a superior fit to be achieved, as shown in Figure 27.

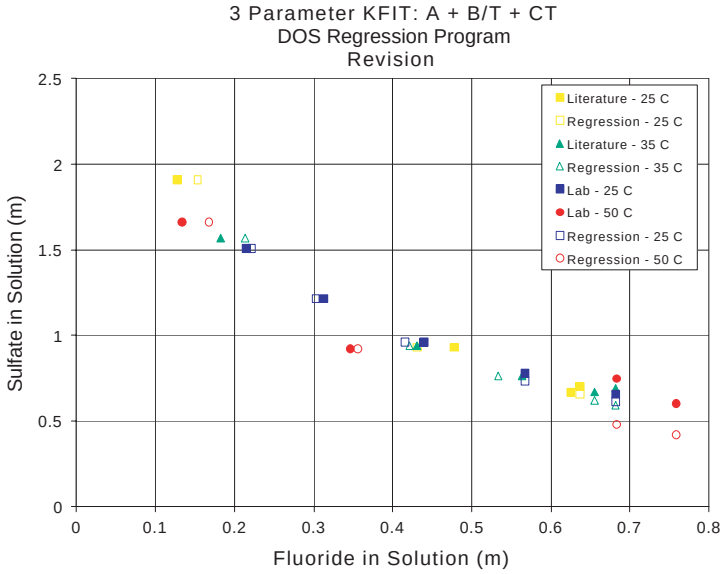

FIGURE 27. Regression results – sodium fluoride sulfate double salt in aqueous solution – DOS-regress program, partitioned data set.

The full experimental data set obtained in the laboratory will be used along with the available literature data to further refine the thermodynamic information used by ESP to evaluate solubility of the

sodium-fluoride-sulfate double salt. Regression of the full data set (including the data points corresponding to 1 and 3-m OH) will allow the interaction parameters to be fit for the ($F\text{-}SO_4$), (F-OH), and/or (SO_4-OH) interactions. This effort will be completed by the end of August 2001.

Experimental measurements for the sodium-sulfate-carbonate-hydroxide system were initiated. Laboratory data for the system in aqueous solution at 25°C and 50°C have been completed and are presently being analyzed. Solutions in 1-m hydroxide are currently being prepared.

Solubility studies on the Na-F-NO_3-OH system. Earlier experimental work in these laboratories has focused on the solubility behavior of Na-F-SO_4-OH (above) and Na-F-PO_4-OH.[22] In both these systems, double salts are formed when sufficient amounts of both fluoride and either sulfate or phosphate anions are present. The solubility curves consist of the solubility of the pure component, the solubility of the double salt, and the solubility of the other pure component. Wastes at Hanford contain copious amounts of the nitrate anion. Knowledge of the solubility behavior of a pure component at different levels of nitrate loadings is expected to be of interest with regard to accurate ESP model predictions.

ESP simulations were performed with version 6.3. The solubility of fluoride and nitrate anions and the solids formed (either NaF or $NaNO_3$) were calculated at hydroxide loadings of 0, 1, 3, and 5 m with nitrate concentrations varying (dependent on temperature and caustic loading) from 0 to about 14 m. Two temperatures, 25 and 50°C, were investigated.

The model predictions provided initial estimates for the preparation of the solutions. Typically, the samples were prepared at 15% (by weight) above the model estimates. All solutions were pre-heated above the equilibrium temperature. Once all of the solids had dis-

solved, the samples were slowly cooled to room temperature, after which the samples were allowed to equilibrate for a period of not less than two weeks. The solutions were mixed by shaking using the shaker table or by hand. Samples were mixed at least once a day following attainment of the equilibration temperature.

Following the equilibration period, the samples were filtered under a vacuum at the equilibrium temperature. An initial dilution of the supernate phase was performed by adding a known weight of water to the collection flask. This prevented the formation of any additional solids, by, for example, a decrease in the temperature of the solution.

Solids were identified using the polarizing light microscope. Figure 28 is an image showing both NaF and $NaNO_3$ crystal phases. In general, the formation of sodium nitrate was restricted to a very narrow compositional range. Liquid phase concentrations were obtained from ion chromatography. Additional water was added to the filtrate to coincide with the linear response range of the IC calibration. The response of the IC was strictly linear from 2 - 30 ppm for fluoride and from 5 - 150 ppm for nitrate. Concentrations in the equilibrated liquid phase were determined from the IC results along with the dilution factors. All dilutions were performed on a weight basis.

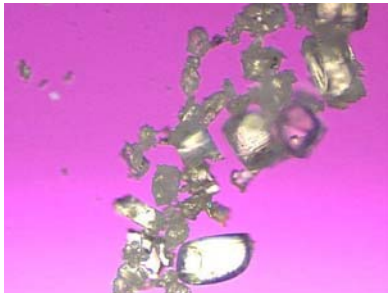

FIGURE 28. Polarizing light microscope image for NaF and $NaNO_3$ obtained during the solubility studies on the Na-F-NO_3-OH system.

Experimental results and ESP predictions for the measurements at 25°C are presented in Figure 29. Both the model predictions and the experimental results reveal a decrease in solubility as the concentration of hydroxide increases. The concentrations of fluoride alone (data on y axis), either in pure water or in any of the hydroxide loadings investigated, are in excellent agreement with the model predictions. Similar comments apply to the comparison of the model predictions with the experimental concentrations for nitrate in water and 1-m hydroxide (x axis). Experimental concentrations are in slight excess of the ESP results in 3-m and 5-m caustic. A close examination of the experimental data for all caustic loadings indicates that the solubility of fluoride is slightly less than the model predictions at intermediate nitrate concentrations.

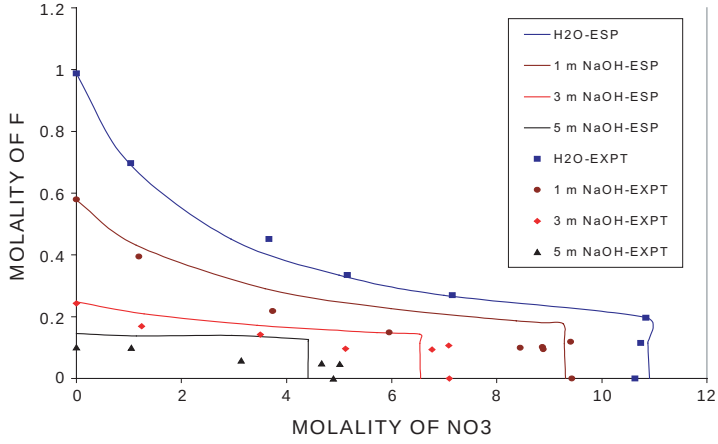

FIGURE 29. Solubility envelope for the Na-F-NO_3-OH system at 25°C. Solid lines are the ESP model predictions and the data points correspond to the experimental measurements.

The fluoride concentrations all show a gradual decrease with increasing nitrate concentrations followed by a region of constant nitrate concentration. In all cases, the solids in the first regime were found to be sodium fluoride. In the region where the nitrate concen-

tration was constant, the only solid observed was sodium nitrate. At the junction of the two lines, both solids were found as shown in Figure 28.

The results obtained at 50°C and the ESP predictions are given in Figure 30. The general trend in the data, similar to that found at 25°C, is the decrease in both fluoride and nitrate solubility as the hydroxide concentration is increased. The concentrations at the elevated temperature are, at all levels of hydroxide loadings, less than those predicted by the model. The fluoride solubilities are all below the model predictions in the range of intermediate nitrate concentrations; this result is also consistent with the lower temperature data. As compared to the data in Figure 29, the experimental nitrate concentrations are found to be less than those predicted by the model. These differences are small, accounting for 5% at most.

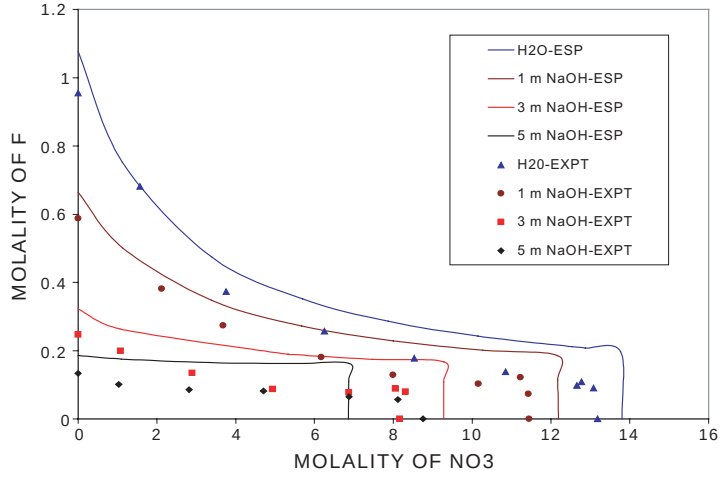

FIGURE 30. ESP predictions (solid lines) and experimental measurements (symbols) for the Na-F-NO_3-OH system at 50°C.

The data obtained at 25 and 50°C in 1-m hydroxide are given in Figure 31. A slight increase in the fluoride solubility occurs with an

increase in temperature. The increase in temperature resulted in a somewhat larger increase in nitrate solubility—both in the experimental data and in the model calculations. The weak fluoride temperature dependence is similar to that observed for the Na-F-SO_4-OH system described above. All of the other data at the hydroxide loadings investigated illustrated similar behavior.

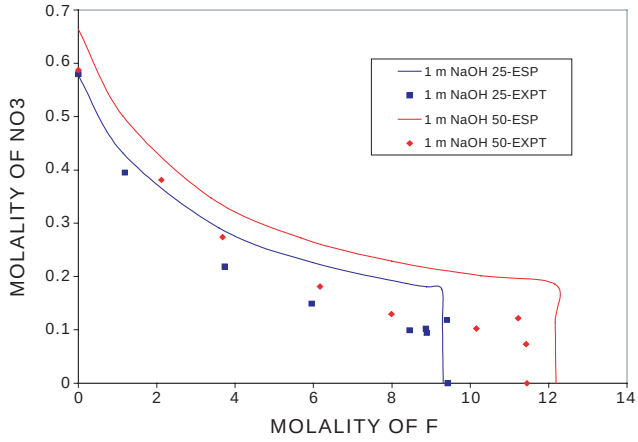

FIGURE 31. Experimental and ESP calculated results for the data obtained in 1-m hydroxide at 25 and 50°C.

Interaction parameters and KFIT expressions are being developed for the data described above.

Conclusion

The high fluoride content in saltcake BY-109 has revealed discrepancies between the ESP predictions and experimental measurements of fluoride, sulfate, and phosphate liquid phase concentrations. Experimental characterization of the BY-109 solids at Hanford will provide necessary information regarding the solid phase partitioning of fluoride in the waste.

Regression of the sodium-fluoride-sulfate double salt solubility data measured in the laboratory has been initiated, and parameters for the ESP KFIT expression have been determined from the aqueous solution data. Interaction parameters between like ions will aid in describing the experimental data obtained in 1-m and 3-m caustic solutions.

Experimental results for the Na-F-NO_3-OH system were reported for both 25 and 50°C. Solubilities for fluoride and nitrate were found to be in good agreement in water at all nitrate loadings. Fluoride concentrations measured at 1-m, 3-m, and 5-m hydroxide at 25°C were slightly less than the concentrations predicted by the model, whereas pure component nitrate anion concentrations were in excellent agreement at all hydroxide loadings. Liquid phase concentrations at 50°C were all slightly less than the model predictions at all levels of caustic loading. A weak temperature dependence of fluoride ion concentration was observed, and a somewhat larger increase in nitrate solubility was found. Determination of KFIT expressions and interaction parameters for this system are in progress.

Project Status

This program is continuing with future efforts aimed at completing the solubility studies on the double salts present in the waste streams at the site and with support of saltcake retrieval demonstrations.

Work Planned

Regression results for the sodium-fluoride-sulfate-hydroxide system and the sodium-fluoride-phosphate-hydroxide system will be completed, including the influence of hydroxide ion. These results will be incorporated as an additional database in ESP and saltcake dissolution simulations for BY-109, TX-113, BY-102, and BY-106

will be revised. The information made available from the BY-109 solids characterization will be used to validate the model predictions. Experimental measurements for the sodium sulfate-carbonate-hydroxide system will be completed. Data bases specific to these systems will be generated and transferred to the site.

References

22. R.K. Toghiani, J.S. Lindner, C. Barfield, and E.C. Beahm. 1998. Saltcake Dissolution Modeling, FY 1998 Status Report, DIAL-40395-TR98-1. Diagnostic Instrumentation and Analysis Laboratory, Mississippi State University, Starkville, MS.

23. R.K. Toghiani and J.S. Lindner. 1999. Saltcake Dissolution Modeling, FY 1999 Status Report, DIAL-40395-TR99-1. Diagnostic Instrumentation and Analysis Laboratory, Mississippi State University, Starkville, MS.

24. J.S. Lindner, R.K. Toghiani and C. Barfield. August 1998. Thermodynamic Simulation of Tank 241-SY-101 Dissolution, Part 1: In-situ Crust Dissolution, DIAL 40395-TR98-1. Diagnostic Instrumentation and Analysis Laboratory, Mississippi State University, Starkville, MS.

25. J.S. Lindner and R.K Toghiani. October 1998. Thermodynamic Simulation of Tank 241-SY-101 Dissolution, Part 2:Supernate Transfer Followed by In-tank Dilution, DIAL 40395-TR98-1.2. Diagnostic Instrumentation and Analysis Laboratory, Mississippi State University, Starkville, MS.

26. J.S. Lindner, J.S. and R.K. Toghiani. April 1999. Thermodynamic Simulation of Tank 241-SY-101 Dissolution, Part 3:Crust Solids Dissolution Modeling and Associated Gas Release, DIAL 40395-TR98-1.3. Diagnostic Instrumentation and Analysis Laboratory, Mississippi State University, Starkville, MS.

27. D.L. Herting. October 1999. Personal communication.

28. D.L. Herting. September 2000. Saltcake Dissolution 2000 Status Report, HNF-7031, Rev. 0. Fluor-Hanford, Richland, WA.

Solids Formation

J. S. Lindner, V. Raju, R. K. Toghiani, and H. Al Habbash

Introduction

Tank farm operations at Hanford include the interim stabilization program, whereby the supernate and interstitial liquor in the single-shell tanks is reduced. Benefits from this process include the minimization of leakage from aging tanks, limiting migration of waste into the soil and temporarily reducing the amount of waste within the tank. The process consists of jet-pumping the liquid in a given tank, obtained through a screen or salt well to a double-shell holding tank and then to an evaporator. Dilution water is added at the pump head. Recently, solids formation and plugging have been noted during transfers from tanks 241-SX-104, 241-U-103, and 241-BY-102.[29] The primary solid responsible for the plugs from the first two tank wastes has been tentatively assigned, through experiments conducted on the waste liquid in the laboratory, as $Na_3PO_4 \cdot 12H_2O$. The plug formed during salt well pumping of BY-102 was believed to arise from sodium carbonate.

Other solids may participate in the plug formation process, which will largely depend on the solid-liquid equilibrium of the species contained in the waste stream. Little information, aside from the laboratory screening experiments, is available regarding the mechanisms of plug formation and, more importantly, the required change in pressure that would indicate the beginning of plug formation. From operations-measured records, the time needed for a plug can be determined, and by knowing the pressures and flow rates, one can estimate the approximate location of the plug. However, prevention of inadvertent plugs may be possible based on a suitable engineering tool that will allow operators to tailor waste transfers.

Development of an engineering tool that can describe slurry transfers and salt well pumping is also an objective of this program. In the case of slurry transport, experimental data are being obtained at Florida International University, and information on solids behavior, size, and growth rates is being compiled at AEA Technologies. A test loop for obtaining data on supernate transfers does not currently exist. The lack of a test loop for salt well pumping, the need to understand the process in greater detail, and a need for the fundamental data for development of the engineering tool provided the basis for the work described below.

Work Accomplished

Results and Discussion

Salt well pumping flow loop experiments

In the previous report we described the behavior of sodium phosphate dodecahydrate particles and agglomerates under flowing conditions in the DIAL saltwell pumping flow loop.[30] For these tests, the velocity of the SX-104 surrogate was set to 8 cm/sec. Images were collected illustrating crystal formation and aggregation and deposition in the channel. Particle dimensions, velocities, and the average bed height for the entire run were determined. Critical (sedimenting) particle dimensions were calculated and compared to those obtained from the images. Based on the above data, the development of the phosphate plug was determined to consist of four events: 1) initial growth of single particles of rod-like or ellipsoidal shape, 2) aggregation of the particles into larger structures associated with bed formation, 3) further aggregation and bed growth, and 4) an increase in the solid fraction in the channel with eventual plugging.

Screening experiments conducted prior to the insertion of the clear plastic tube in the flow loop and the subsequent adaptation of the DIAL imaging system resulted in a time to plug of 255 seconds at

the 3.5 gph (8 cm/sec) flow rate. Plug formation at a flow rate of 6.8 gph (15 cm/sec) took upwards of 3,000 seconds. Additional experiments were therefore conducted to compare the behavior of the surrogate under the two conditions.

The surrogate used in these experiments was derived from the Best Basis Inventory compilation for the supernatant from Hanford tank 241-SX-104.[30] The composition consisted of the sodium salts of aluminate, nitrate, hydroxide, phosphate, and carbonate, in the proportions of (1, 7, 2, 0.3 and 0.1 moles respectively), and water (55.5 moles). The salt well pumping flow loop was described in the previous report.[30] In brief, the channel diameter was 0.25 in. and an immersion heater in the stainless steel holding tank controlled the temperature of the surrogate prior to flowing in the channel. A tube-in-shell heat exchanger was used to decrease the temperature of the surrogate from 46˚C to around 40˚C. The higher temperature was originally attained from natural convection of the surrogate solution as it flowed into the upper portion of the 10-ft long channel. Corrosion resistant thermocouples and pressure transducers were employed and were interfaced with a data acquisition system. Data were logged at 1-second intervals and eventually transferred to a spreadsheet file for further analysis. Images were collected, at a rate of 25 frames/2 seconds, using the DIAL imaging system with a lens combination at an effective focal length of 150 mm. Single particles, agglomerates, and the fractional bed area were analyzed using the software associated with the polarizing light microscope.

Recorded temperatures and pressures for the experiment with an initial velocity of 15 cm/sec are shown in Figure 32. Data are shown from immediately prior to activation of the heat exchanger until cessation of flow. As in the lower (3.5 gph) flow-rate experiment, the flow of water to the heat exchanger was maintained at 1.2 gpm.

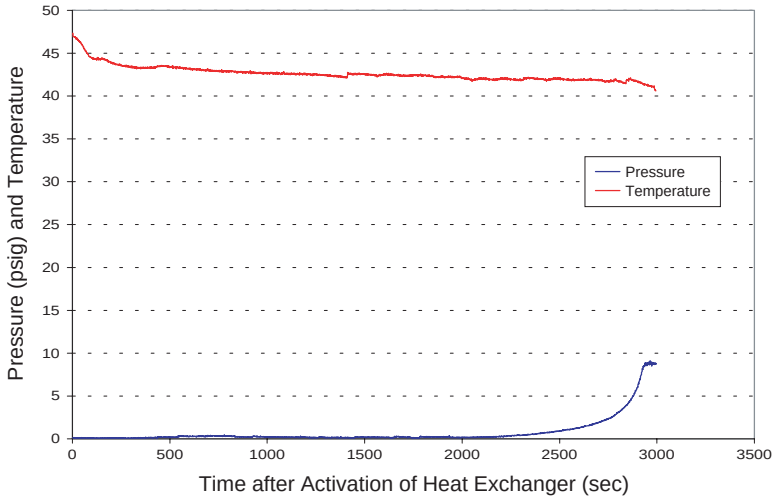

FIGURE 32. Process data for the flow loop experiments at 15 cm/sec.

The temperature of the SX-104 supernatant surrogate in the holding tank was maintained at an average of 50˚C. Cycling of the upstream temperatures, consistent with the operation of the immersion heater, was observed. This effect was not seen in the lower flow-rate experiments, owing to the short duration (6 minutes) of those tests.[30] For the data in Figure 32, any upstream temperature cycling was effectively damped out in the clear section of the channel.

Previous work has indicated that the sodium phosphate dodecahydrate crystals are not observable with the spatial resolution of the imaging system prior to 190 seconds, with eventual plugging occurring at 225 seconds. Similar results were obtained here. The first particle observed from the collected images was found 2,550 seconds after activation of the heat exchanger. The induction time was increased due to the higher velocity of the surrogate waste fluid and the less effective heat transfer from the surrogate to the cooling water. Plug formation occurred around 2,923 seconds.

Images collected during the experiment were similar to those observed during the low-velocity experiment.[30] The width and length dimensions of the particles were quantified, and a comparison of the ultimate particle areas for both experimental runs is shown in Figure 31. Here, the ordinate has been taken as starting from the observation of the initial particle. The data illustrate the initial formation of single crystals followed by the formation of larger aggregates along with the single particles and, finally, the dominance of aggregate formation during the later stages of the process.

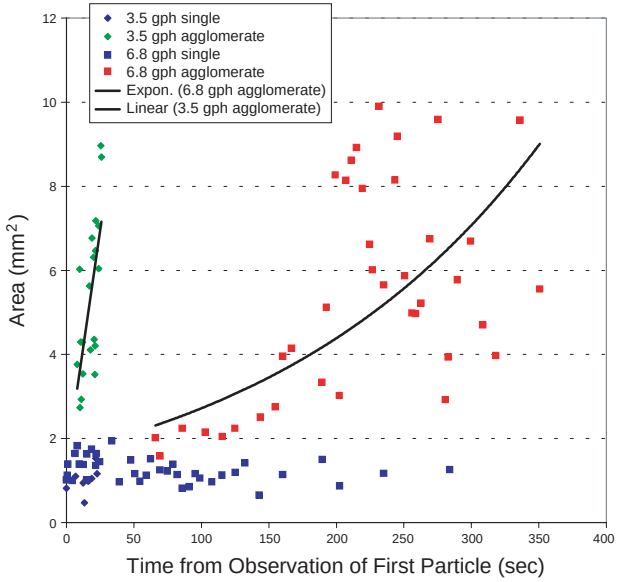

FIGURE 33. Reduced time plot of the single and agglomerate particles observed during flow loop experiments at 8 and 15 cm/sec (3.5 and 6.8 gal/min, respectively).

Calculated particle growth rates were also similar to those found in the low-velocity experiment. For the run with an initial velocity of 15 cm/sec, the single particles grew at a rate of 2 ± 0.9 mm^2/sec. For the 8 cm/sec experiment, the single particle growth rate was 2 ± 0.5 mm^2/sec. The agglomerate growth rate for the higher-velocity experi-

ment was 19 ± 11 mm^2/sec, while at the lower velocity or lower Reynolds number, the average growth rate was 14 ± 8 mm^2/sec. The higher deviations probably arise from the larger number of particles observed during the higher-velocity experiments. The formation of the moving bed and the eventual plug occurred at longer times, permitting the larger sample. The larger velocities measured in the 6.8gph run imply larger critical dimensions.

The critical velocity, V_{crit}, is defined as the velocity at which a particle begins to sediment in the channel.[31]

$$V_{crit} = (V^2/2gW^*)\{2gd((\rho - \rho_i)/\rho_i)\}^{0.5} \quad \textbf{(EQ 2)}$$

Here, g is the gravitation constant accounting for the force normal to the direction of flow, V is the stream velocity, W^* is a critical particle dimension, taken here as the particle width, d is the channel diameter, and the ρ values account for the particle and carrier fluid densities. In both experiments, the velocity of the flow continues to decrease once the particles and agglomerates begin to form. Consequently, the critical dimension will continually decrease. The extent of sedimentation will depend on the change of velocity with time and the associated size and growth rates of the particulates.

Figure 34 provides the calculated critical widths and the widths measured during image analysis against the measured velocities. The plot contains data pertinent only to the single particles. Some of the measured particle widths for the lower-flow-rate experiment (3.5 gph) are very close to the calculated critical widths as they underwent sedimentation during that run.[30] In contrast, the particle widths determined from the images for the higher-velocity run (6.8 gph) were all smaller than the calculated critical dimensions. The particles' growing to only a finite size (Fig. 33) implies that bed development occurs through particle agglomeration at velocities greater than about 9 cm/sec (the estimated intercept of the particle size and calculated critical particle size).

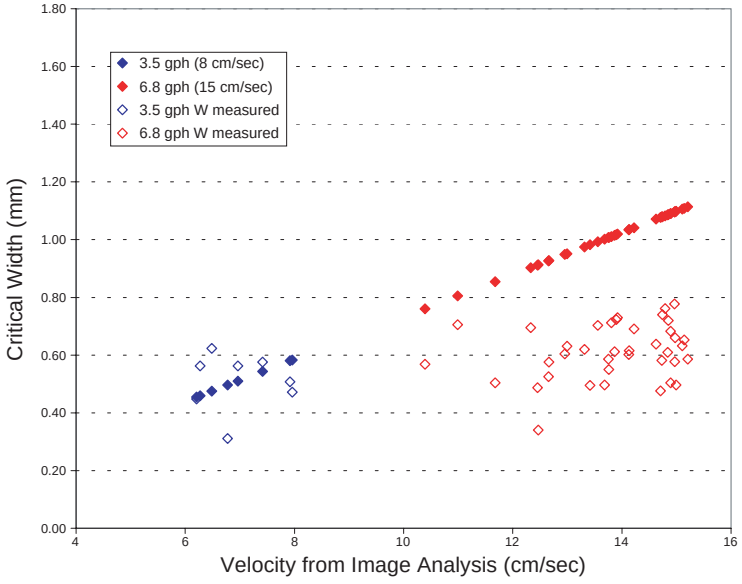

FIGURE 34. Calculated critical widths (solid symbols) and measured widths (open symbols) for the 3.5 and 6.8 gph flow loop experiments.

Reduced particle velocities, determined by dividing the measured particle velocity by the initial particle velocity, are plotted against the bed area fraction in Figure 35. Changes in the normalized particle velocity with bed area are similar for both data sets. A number of slope changes can be assigned. Initially, the particle velocity decreases; however, little accumulation occurs. The next (second) region, which may contain two slope changes, reflects a more gradual change in velocity as additional sedimentation occurs. There appear to be two distinct slopes in this regime: the first occurring from around a bed fraction of 0.1 and extending to about 0.6, and the second from about 0.6 to 0.95. The fraction of 0.6 probably reflects the change from bed development to a moving bed flow. The last regime is not observed but occurs when the bed fraction increases from 0.95 to 1.0. The velocity decreases rapidly in this region; however, the par-

ticle velocity was not obtainable due to optical interference from the developed bed.

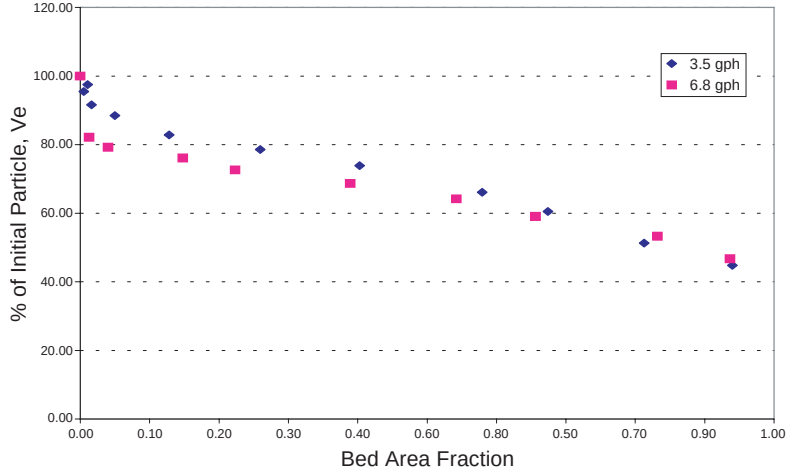

FIGURE 35. Correlation of the reduced particle velocity with the measured bed area fraction.

The data indicate that the particles behave similarly at the different flow rates. The growth of the bed is also similar (Fig. 36). Here, the run time has been normalized to the time at which the plug formed. The pressures are super-imposable, indicating the similarity in the particle growth, aggregation, and bed-formation processes. In examining the data in Figure 33 along with the temperatures presented in Figure 36, we observe that the temporal delay in plug formation at the 6.8 gph flow rate, as compared to that at 3.5 gph, is accountable by the higher velocities. At the same cooling rate (1.2 gpm), the heat extracted from the surrogate flow is less at the higher surrogate velocity.

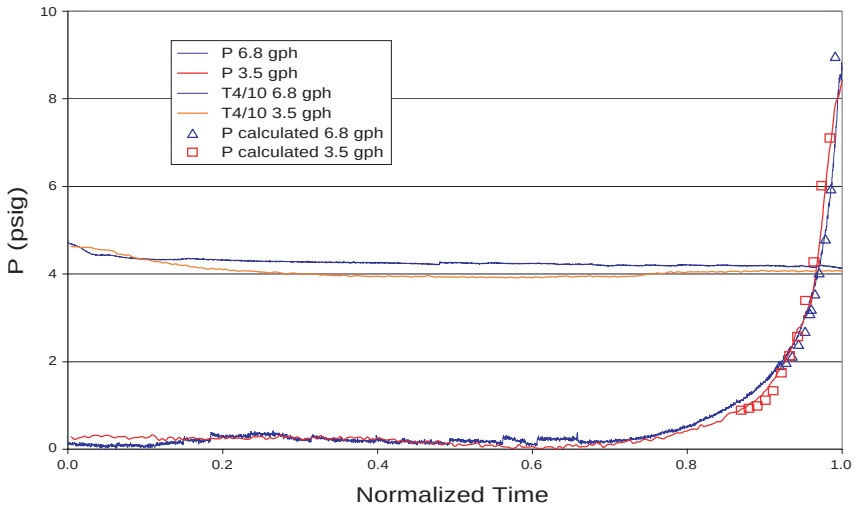

FIGURE 36. Saltwell pumping flow loop data for the 3.5 and 6.8 gph experiments. The time axis has been normalized to the time at which the plug formed.

Application of models to describe the transport of the SX-104 supernatant surrogate

The symbols in Figure 36 correspond to the pressures calculated for a two-phase flow according to the model of Wilson.[32,33] The model considers that the particle bed is comprised of dense solids and that the liquid is isotropic. The bed height, as determined from the collected images, is then used to determine the solid fraction and the liquid fraction by subtraction. The liquid and solid layers are assumed to share a common pressure. As the solid fraction is amassed within the channel, the corresponding pressure increases. Full details of the calculations can be found in the references [32,33]. Good agreement with the model was found.

In all experiments thus far (see, for example, Figs. 32 and 36), the downstream fluid temperatures show a rapid decrease from the initial 46˚C value immediately following the activation of the heat

exchanger. A gradual decrease then occurs, followed by a near-constant temperature. The reason for the increase in the downstream temperature for the run at 3.5 gph (Fig. 5, temperature scale compressed) at a reduced time of around 0.8 is not known; however, the large majority of data indicate that a constant temperature is approached.

Particles were first observed in the 3.5 gph run approximately 196 seconds into the run with eventual plug formation at 230 seconds. Similarly, in the 6.8 gph experiment, the first particle was observed at 2,550 seconds with the plugging at 2,930 seconds. The reduced times for observation of the first particles were 196/230 or 0.85 for the 3.5 gph run and 2550/2930 or 0.87 for the experiment at 6.8 gph. For a long portion of the run, the predominant mode of heat transfer is convection. Formally, the presence of particles in the fluid would imply that both convection and conduction are important. In these experiments, however, the role of conduction appears to be minimal. First, the temperatures are essentially constant during the latter portions of the experiments; second, the formed plug behaves more as a gel than a pure solid. Previous ESP model calculations have indicated significant liquid volume fractions at these temperatures.[30] The thermal profile of the fluid during the experiment corresponds to unsteady convection.

A number of models are available for unsteady convection problems. In this work, we have found that the model of Krishan best describes the observed behavior.[34] The formalism accounts for a step change in the heat applied to the channel and solves the associated energy expressions using term-by-term inversion. The model was implemented using math software. Data were then fit to expressions and compared to those expressions obtained for the experimental temperatures using the same function equation form. The experimental data and the model predictions (symbols) are shown in Figure 37.

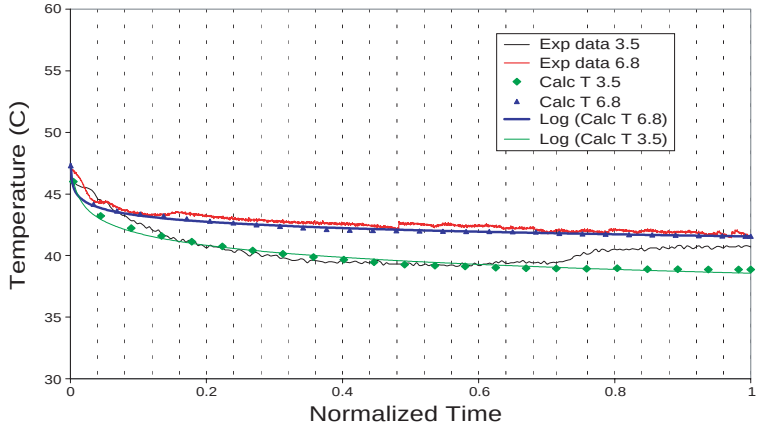

FIGURE 37. Downstream temperatures determined during the 3.5 and 6.8 gph experiments and the downstream temperature calculated from the heat-transfer model of Krishan.[34]

The functional form of the model and the experimental data can be given by $y = a\ ln(x) + b$, where x is the reduced time. Associated constants and correlation coefficients are collected in Table 2.

TABLE 2. Calculated slopes, intercepts and correlation coefficients for the data from Figure 37.

Flow Rate (gph)	Origin	a	b	r(1)
3.5	T4 Experimental Data	-1.41	38.6	0.994
3.5	Model Prediction	-1.25	39.3	0.81
6.8	T4 Experimental Data	-0.85	41.8	0.997
6.8	Model Prediction	-0.74	41.6	0.981
(1) The correlation coefficient has been reported here as r and not r^2.				

The unsteady-state heat transfer model describes the data well. Both the slopes and the intercepts are similar for a given experiment. The slopes are within 14% of the model predictions. The large difference is partially accountable by the (non-standard) increase in T4

observed during the 3.5 gph run. Intercepts are within 0.8%, indicating that the model accurately predicts the final temperature of the fluid. Of interest in the model predictions and the experimental data are the intercepts that represent the final temperature achieved. The ratio of the "a" values for either the model calculations or the experiment yield an average of 1.68. This value can be compared to the ratio of the velocities or the flow rates for the two runs, which was determined as 1.90. The corresponding error is around 12%. Further evaluation of the heat transfer model with other data is in progress.

Feed stability and prevention of solids formation model(s)

Of the six existing cross-site transfer pipelines between the 200 West and 200 East areas of the Hanford Site, none is considered capable of transporting waste slurries with significant solids loadings. Five of the six lines are considered unusable due to plugging or similar problems. The sixth line is used only for liquid waste transfer due to design limitations and age.[35] A new, replacement cross-site transfer system (RCSTS) was constructed to replace the existing pipelines.[36] This replacement pipeline was designed according to the Hanford Site Tank Waste Remediation System (TWRS) waste compatibility program, which requires that all precautions be taken to prevent line pluggage during waste transfers.

The design and analysis of the RCSTS were based on semi-theoretical or empirical correlations using waste properties obtained from tank waste characterization tests. These correlations calculate minimum slurry transport velocities needed to maintain suspensions of solid particles in slurries, given the knowledge of a sufficient amount of slurry physical properties. This transport velocity is also known as the slurry flow critical velocity.[37] It is not universally recognized that a transfer line flow velocity in excess of the critical velocity is a requirement to prevent solids deposition and possible line plugging. However, slurry critical velocity seems to be the most prevalent objective measure to prevent solids from deposition in transfer lines.

This is also supported by the fact that precipitation of solids, which may result in gelation and promote settling of particles, has been speculated to be the main cause of plugging in the existing cross site transfer system pipelines. The advantage of these critical-velocity correlations is that their use is not reliant upon any measure of bulk slurry viscosity. The input parameters are limited to slurry phase densities and mass fractions, pipeline diameter, particle diameter, and viscosity of the carrier fluid of the slurry. Consequently, the critical velocity calculations do not require determination of the system pressure drops. Generalized slurry properties, therefore, can be recommended if the slurry can be adequately described by these variables and if the carrier fluid viscosity is known. The disadvantage of these correlations is that they were developed for specific systems of slurries that involve components such as sand or coal, which do not necessarily represent the Hanford waste slurries.[37]

From a fluid-mechanics point of view, the slurry transport of Hanford tank waste is a challenge because of the compositionally complex and diverse nature of its contents. One of the major complexities is that much of tank waste contains appreciable amounts of insoluble submicron particles.[37] These fine particles may stick together, forming larger-size agglomerates.[37] Additionally, these larger agglomerates may network to form gel-type materials that might plug the transfer lines. Agglomeration kinetics are sensitive to the pH value, temperature, or salt concentration. Since no simple engineering correlation exists to express this effect during slurry transport, most of the critical velocity analysis is based on simplified slurry properties.

Numatec Hanford Corporation (NCH) and Lockheed Martin Hanford Corporation (LMHC) have raised concerns that the RCSTS may not meet pumping requirements for all proposed future waste slurry transfers.[37] This prompted researchers to perform more studies on the RCSTS, some of which has suggested that the current tank farms waste compatibility program criteria may be insufficient to prevent particulate solids from settling within slurry composition ranges cur-

rently allowed by the waste compatibility program. However, in order to relate a critical velocity associated with a certain slurry composition to a system limit, a means of relating the system capabilities to the slurry composition must be found. Generally, this means expressing the bulk or effective viscosity of the slurry being transferred to some more readily obtainable variable, such as slurry density or solids concentration. No universally recognized model exists to accomplish this, and there is a great uncertainty among results from those models that do exist.[37]

As a result of the critical-velocity correlations studies, a recommendation was made to require a special engineering evaluation prior to any waste transfer that involves particulate solid transport. This evaluation is needed to gain a measure of confidence that the critical velocity for a given slurry composition is within the capabilities of the transfer system.

It is important to know that most, if not all, of the critical velocity correlations rely on a one-dimensional analysis of the flow field. This does not provide a reliable estimate for pressure losses through the piping system, especially for waste slurries of the Hanford type. A more general approach using two- or three-dimensional analyses should provide a better understanding of the problem and help validate those critical velocity correlations. Computational Fluid Dynamics (CFD) is one of the options that can provide that type of general approach to analyze the complicated problem at hand. The only drawback is that a full-scale CFD simulation will require considerable preparation and processing time for one specific waste composition and particle size distribution (PSD). A more economical approach would be to perform a series of CFD simulations with slurry properties that represent the bounding upper and lower limits for Hanford waste. These simulations will then be analyzed and the results compiled to produce an operating envelope or surface that can be used by the site operators. This should help to determine whether a waste-slurry pumping operation can be done safely—without forming a

plug—and with the available RCSTS capabilities (available pump head, max pressure, etc.), without exceeding its limits.

Prior to performing the full scale CFD work, we performed a parametric study to determine the sensitivity of slurry flow to the waste properties.[30] The effects of flow velocity, solids density, volume fraction and PSD, and waste viscosity on the transport of slurries were studied. The results showed the importance of flow velocity, solids density, and slurry viscosity, clearly indicating that accurate values are necessary to obtain accurate results. The effect of particle size distribution was not as important, although the size and amount of the larger particles in the PSD are. This is because the flow velocity should be able to suspend the largest particles if sedimentation is to be prevented.

Project Status

Work on both aspects of this project, salt well pumping experiments and the development of the engineering tool, are continuing.

Conclusions

Additional saltwell pumping flow loop experiments have been conducted on the base SX-104 supernatant surrogate composition. These experiments were conducted at an initial velocity of 15 cm/sec, as opposed to those results reported earlier, which corresponded to an initial 8 cm/sec flow. Particle dimension and growth rates were similar for both experiments. The longer time necessary to form the plug in the current experiments corresponds to the higher velocities of the flow. In this case, the critical particle dimensions are below those necessary for the particle sedimentation until the velocity has been reduced by around 30%. Comparison of the data for both runs indicated similar pressure and relative velocity profiles when the run time was normalized to the time at which the plug formed. Models were

applied for the increase in pressure and for the unsteady heat-transfer problem associated with the experiments. Calculated results were found to be in good agreement with the experimental data.

Development of a path for establishing a three-dimensional contour plot that allows operator decisions on site waste transfers is detailed. The work considers the primary characteristics of the slurry waste and will be compared to existing correlations. The approach will involve extension of the previously reported sensitivity studies and establishing limits on the physical properties of the waste, such as densities, solids loadings, and viscosities.

Work Planned

Additional work is needed to apply the models for pressure and heat transfers to data taken previously. Experiments on surrogates with different phosphate loadings are in progress to establish the dependence of plug formation on phosphate loading. Efforts to develop and evaluate chemical treatments for plug remediation have been initiated. Further studies on development of the engineering tool will focus on completion of the sensitivity study and at the validity of the underlying assumptions employed in empirical representations of slurry transport.

The main goal of the remaining work for FY 01 is the development of a three-dimensional operating surface that describes slurry waste transfers at Hanford for a given (or assumed) PSD and solids volume fraction. The three major axes in the three dimensional space would be the velocity, density, and viscosity. The points on the surface will be generated by performing simulations (for the given PSD and volume fraction) at different but bounded combinations of velocities, densities, and viscosities. The choice of variables on the axes was based on the sensitivity analysis performed earlier.

References

29. D.A. Reynolds. May 2000. Status of waste transfers, criteria, and plans. Presented at the Third Saltcake Dissolution and Feed Stability Workshop, Richland, WA.

    J.R. Jewett. January 2000. “Tank Farm Information for TFA Workers” and ”Saltwell Pumping from Tank SX-104”. Numatec Hanford Corporation, Richland, WA. Personal communication.

30. J.S. Lindner, H. Al-Habbash and R.K. Toghiani. 2001. Prevention of solids formation. *Instrumentation Development, Measurement, and Performance Evaluation of Environmental Technologies.* Technical Progress Report DIAL 40395-11, January - March 2001. Mississippi State University: Diagnostic Instrumentation and Analysis Laboratory.

31. See, for example, E.J. Wasp, et al. 1977. Solid-liquid flow slurry pipeline transportation. *Series on Bulk Materials Handling.* Clausthal, Germany: Trans Tech Publications, 1:4.

32. K.C. Wilson, et al. 1996. *Hydraulic Conveying of Solids with Centrifugal Pumps.* London: Chapman and Hall.

33. D.J. Mason and A. Levy. 2001. *International Journal on Multiphase Flow,* 27:415-435.

34. B. Krishan. 1982. *International Journal on Heat Mass Transfer.* 25:288.

35. J.D. Hudson. April 1996. Defining waste acceptance criteria for the Hanford replacement cross-site transfer system. PNNL-11146/UC-2030. Pacific Northwest National Laboratory, Richland, WA.

36. A. Shekarriz, Y. Onishi, P.A. Smith, M. Sterner, D.R. Rector, and J. Virden. April 1997. Cross-site transfer system at Hanford: long-term strategy for waste acceptance. PNNL-11487/UC-2030. Pacific Northwest National Laboratory, Richland, WA.

37. S.D. Estey. October 1998. Flow velocity analysis for avoidance of solids deposition during transport of Hanford tank waste slurries. HNF-2728. Lockheed Martin Hanford Corporation, Richland, WA.

TASK 4

Environmental Control Device Testing

Evaluation of HEPA Filter Performance

J. A. Etheridge

Introduction

In 2000, the U.S. Department of Energy (DOE) and the Environmental Protection Agency (EPA) signed a Memorandum of Understanding to combine research efforts to the maximum extent possible to resolve important questions of common interest. One of these revolved around the issue of assuring the performance of HEPA filters used in off-gas systems. As a result, this Technical Working Group was chartered to provide methodology to ensure that HEPA filters provided adequate protection throughout their service life. The work proposed here is a direct result of the efforts of the NTW.

One of the major parts of this project is a survey of what has already been done, what is currently being done, and what the priorities are for additional work that needs to completed. At present there is a lot confusion and misinformation concerning HEPA filters, filter testing, and filter applications. There appears to be a strong need for a HEPA filter test bed for the purposes of challenging the filter medium as well as for development of instrumentation. We plan to construct a

filter test bed (HEPA Filter Challenge Facility). It will be capable of DOP/PAO testing as well as handling a variety of other challenge agents including water, smoke, heat, and particles from particle generators. It will be instrumented and monitored in much the same way as the combustion test stand and will also be useful for instrument development and CEM testing. Modeling of the results of specific types of failures will also be done along with testing, where practical, to verify that the model is useful. This is important for understanding both DOP testing and online failure of HEPA filters.

One of the major needs related to HEPA filters is the need for a "break through" detector. Testing of the cavity ring down system for possible use as a break through detector is also planned. It is also proposed to acquire an "electrostatic impactor" (ELPI) for use as both a measure of input challenge agents and for measuring after the HEPA filters. If this unit is successful in measuring very low particle concentrations (or low mass loading) it will allow us to test the limits of detection of other particle measuring techniques.

The scope of this project could be amended depending upon the results of the NTW's review of our Data Quality Objectives and the evolution of the NTW's HEPA Filter Performance position paper. However, it is believed that the activities described below accurately represent the magnitude of the effort, and the equipment and supplies required for the program.

Work Accomplished

Work on determining the scope of work to be done in regard to HEPA filter testing and measurements has continued through a number of conference calls with the NTW members. It was decided to take advantage of the fact that a number of the NTW members were planning to attend the IT3 Conference in Philadelphia by scheduling a HEPA project meeting at the conference. This was a very productive meeting that helped set the goals and scope of the project.

Work Planned

Enough progress was made for us to begin work on a test plan for the HEPA project. Work on the Test Plan has already begun with some of the introductory sections being essentially finished. A first draft of some of the more technical sections of the test plan is scheduled to be sent to members of the NTW for review and comments in July. Once all sections are completed and reviewed by the NTW the Test Plan will be subjected to peer review by the ASME.

Sampling System for Dioxins, Furans and Other Semi-volatile Products of Incomplete Combustion and Characterization

C. Waggoner and C. B. Winstead

Introduction

Selected congeners of the families of dioxins and furans (D/F) are potentially some of the most carcinogenic compounds known to exist. Recognition of the potential risk to the U.S. population spurred the conduction of a national inventory of D/F sources. A significant outcome of this initiative has been the establishment of a strategy to reduce emissions in a targeted fashion. One of the centerpieces of the D/F reduction strategy is the Maximum Achievable Control Technology (MACT) standard just issued for hazardous waste combustors (HWC). Each of the DOE hazardous or mixed waste incinerators falls subject to this new standard and there are stringent emission levels that will need to be met in the near future.

The 0.2 ng/dsm^3 emission standard called for under the HWC-MACT stresses the technical limits of operational control and emissions testing. Uncertainties associated with US EPA reference

method stack sampling accuracy and method quantification limits for the 17 D/F congeners that have non-zero toxicity equivalence factors invite skeptical review of the measurements that will be made by facilities to demonstrate compliance with this new standard.

Of the six needs listed on the DOE EM-Needs web page related to dioxin/furan problems, three (ID-3.2.32, ID-S.1.02, and SR00-1021) recognize the lack of knowledge associated with the specific locus of D/F formation, the distribution of D/F congeners between adsorbed and gaseous phases at temperature, and/or the behavior of these classes of compounds in the sampling train. This lack of knowledge is an impediment to minimizing emissions by process control or design/operation of pollution control devices. Additionally, a much fuller understanding of the phase behavior in off-gases is essential to development of a functional continuous emission monitor or verifying the accuracy of extractive sampling methodologies. Finally, a clearer picture of the gas phase chemistry is the best hope of identifying a dependable analytical surrogate, if one exists.

Intensive research has been undertaken throughout the past two decades to gain a more complete understanding of the mechanism(s) of dioxin/furan formation in combustion processes. The majority of controlled mechanistic studies of D/F formation tend to be carried out using bench top and micro-scale apparati. A significant body of data has also been accumulated from off-gas samples collected from solid waste incinerators and industrial processes. However, the large number of variables associated with fuel feed and operational history of incinerators makes it difficult to extrapolate from bench to full scale. A series of studies is proposed to take advantage of bench scale results and, in a two-stage manner, extend these investigations to pilot scale.

The primary focus of this effort will be to determine the behavior of D/Fs associated with fly ash particulates in an isothermal off-gas environment for the temperature range of 300 to 800˚F. This will

include analysis of samples for D/F homologues to determine the extent of formation, destruction, and dechlorination under test conditions.

All of the results from these investigations will be utilized, along with literature information, in the initial development and evaluation of a hybrid artificial intelligence system (combination neural network-expert system) to project D/F formation, identify areas of needed research, and search for analytical surrogates.

Work Accomplished

Various parts of the DIAL sampling system have been constructed and evaluated over the past quarter. The minimal void volume filter housing for hot filtration of particles has been fabricated. A variety of trap configurations have been developed and evaluated with respect to volumetric flow rates and pressure drop. Peltier coolers have been evaluated with regard to heat removal capacity. An extensive search has been conducted to identify appropriate valves to use on the sampling system, and finally, a heated transfer line used to connect the heated filter box to the trap has been designed and acquired.

Currently the most problematic aspect of developing this sampling system is location of valves. The valve used upstream of the heated filter must have a a straight flow path of one half inch diameter to avoid retaining particles via impaction. Additionally, this valve and seat must be made of a material capable of being coated with an inerting material such as those offered by Restek. Finally, the unit cannot employ a lubricant. Other valves that are used in the system, particularly at the trap, must have void volume as close to zero as possible in order to keep the void volume of the trap to no more than five milliliters. An ideal set of valves has not been identified, however, selections have been made for evaluation purposes. A search continues to locate valves that have a minimal void volume, are fabricated from a

material that can be coated with an inerting material, have a straight flight path to avoid deposition of PM, do not use a lubricant on the valve assembly, and will withstand a temperature of greater than 350˚C.

A set of four 80 watt Peltier thermo-electric cooling units have been obtained and evaluated for temperature control of the analyte trap. A variety of tests have been conducted to determine the adequacy of these units and it has been determined that additional cooling capacity will be necessary. 150 watt versions of these devices have been obtained and water cooled heat sinks required by these units have been fabricated. Thermal properties of this new system is currently under investigation

In order to maximize the concentrating capability of the sampling system, the total void volume of the trap needs to be reduced to as near five milliliters as possible. The length and width dimensions of the trap are dictated by the Peltier cooling units (50 x 100 mm) so the shape and thickness of the trap cavity are the variables that can be manipulated in developing the optimum trap geometry. The tubing that connects the trap inlet to the sampling system and outlet to the impingers and pump needs to be at least one eight inch in diameter so the trap cavity must be mated to this dimension. Three prototype trap units have been fabricated to evaluate the pressure drop across the unit and to determine the functionality of water cooled Peltiers for temperature control. Pressure drop tests indicate that the one eight inch tubing needs to be shortened and/or increased in diameter. The Peltier electronic cooling units are being evaluated for performance with these traps.

The low mass particle feeder that has been developed for use on this project has been modified to make its feed rate more consistent and the unit more portable. An updated control system is also being developed to make the feed rate more variable and to allow interfacing with a computer. Delivery of ash from the feeder to the test stand

is accomplished using a stream of compressed air/nitrogen. The flow rate of this carrier gas is currently too large and in the delivery system is being resized to minimize the volumetric flow rate of the carrier gas while maintaining a transport velocity of the particulate material.

Work Planned

DIAL will continue to develop its small-scale test stand for D/F research and the evaluation of its isokinetic and isothermal sampling system. During the next three months emphasis will be placed on completion of characterization of the sampling system components with respect to thermal and flow properties. The search will continue to identify a set of valves necessary to complete the system ensemble and allow testing of the assembled system. Efforts will also be directed toward reducing the carrier gas flow rate for the particle feeder to a level that is functional with regard to particle transport and nominal with regard to perturbing the off gas chemistry and temperature profile in the region downstream of particle injection.

References

38. K.L. Froese, O. Hutzinger. 1997. *Environmental Science and Technology* 31:542-547.

39. A. Addink, H.A.J. Govers, K. Olie. 1998. *Environmental Science and Technology* 32:1888-93.

40. P.M. Lemieux and J.V. Ryan. 1998. *Waste Management* 18:361-370.

41. P.H. Taylor and B.J. Dellinger. 1999. *Analytical and Applied Pyrolysis* 49:9-29.

42. F. Iino, T. Imagawa, M. Takeuchi, M. Sadakata 1999. *Environmental Science and Technology* 33:1038-43.

Organic Compound Monitoring Using Cavity Ringdown Spectroscopy

C. B. Winstead

Introduction

Several US DOE science and technology needs are based upon the need for high-sensitivity and robust monitoring devices for various organic species. For example, the following needs are all related to the monitoring of volatile or semi-volatile organic compounds (VOCs or SVOCs) in combustion or thermal treatment systems.

- Continuous Emissions Monitor for Offgas Analysis (ID-2.1.18, Priority 1)
- Develop Thermal Treatment Unit Offgas CEM Monitors. (ID-3.2.32, Priority 2)
- Volatile Organic Compound Monitoring and Detection (ORHY-04, Priority 3)

The effort reported here is a continuation and combination of two separate tasks from DIAL's previous cooperative agreement (Task 1.1 *Volatile Organic Compound Monitors Using Diode Lasers* and Task 1.3 *Sensitive Detection of Toxic Chlorinated Compounds*). Together, these projects have demonstrated the first sensitive detection of VOCs such as benzene and chlorobenzene using diode laser CRDS and obtained the first CRDS spectra for dioxin (an SVOC). While the emission of dioxins and furans is an important risk and regulatory consideration, significant research will be required prior to full development of a dioxin/furan continuous emission monitor (CEM). Questions such as how dioxin is partitioned in the gas stream between gas and particulate phases must be investigated and appropriate sampling systems developed before truly quantitative analysis can be carried out on-line. In addition, monitoring dioxin precursor or indicator

molecules such as chlorobenzene may prove to be a viable alternative to dioxin monitoring.[43] Thus, it is beneficial for the development of VOC or SVOC monitors for thermal applications to be coupled with an overall investigation of formation and monitoring of dioxin. Such instruments likely will have value in research efforts to understand dioxin formation well before reaching a level associated with an industrial CEM, a role that may ultimately prove more important for reducing dioxin emissions than a commercial CEM.

The approach taken here includes continuing the development of advanced CRDS techniques using both ultraviolet pulsed and near-infrared diode lasers for the detection of VOCs and SVOCs at atmospheric or reduced pressures. CRDS is based upon the measurement of the time required for light to decay in a stable optical cavity.[44] This light may be injected into the cavity using either pulsed or continuous wave lasers. A small quantity of an absorbing species present in the optical cavity will absorb and thus remove some light from the cavity, reducing the decay time. This change in ringdown time can be directly related to the number density of absorbing atoms or molecules in the cavity. The extreme sensitivity of the CRDS techniques is achieved due to the extremely long effective pathlength (up to several kilometers) for the light recirculating in the cavity to interact with a sample gas.

The efforts described here are focused on improving the sensitivity and selectivity of our previous measurements and participating in collaborative efforts to develop appropriate sampling systems for dioxin species. Slit jet expansion techniques will be incorporated with CRDS to cause narrowing of molecular spectra by decreasing the population in excited vibrational and rotational energy levels.[45] This narrowing will reduce the spectral overlap between different VOCs or SVOCs, thus enhancing detection selectivity. The slit jet expansion will initially be tested with VOCs prior to a demonstration of the detection of dioxin. The expansion cooled spectra will be directly compared to our other room temperature dioxin data to quan-

tify the change in detection limit due to the expansion. These efforts are designed to be complementary to those underway by EPA researchers who are using resonantly enhanced multiphoton ionization (REMPI) for dioxin detection.[46] Continued development of CRDS should ultimately provide a technology complementary to the REMPI system. CRDS sensitivity should not be strongly impacted by increasing chlorination of dioxin molecules, in contrast to expected sensitivity reductions for REMPI.

Finally, small yet ultra sensitive sensor systems could no doubt play a significant role in monitoring and/or process control for a number of remediation activities related to clean-up of volatile organics. For example, a number of subsurface and ground-water remediation efforts could benefit from on-line "process" monitoring for VOCs. These include efforts utilizing soil heating, in-well vapor stripping, passive soil vapor extraction, and other in-situ clean-up technologies where simple, real-time VOC monitoring could be used to indicate or monitor system performance. Low-power sensing technologies for VOC monitoring will be required for long-term monitoring efforts both for atmospheric and subsurface monitors, e.g. for continuous monitoring of subsurface reactive barriers or VOC plumes. Systems have already been demonstrated that utilize underground piping to collect soil gas and transport it to a surface monitoring system.[47] For long-term monitoring, diode-based VOC monitoring systems could significantly simplify the analytical equipment required for monitoring while reducing power consumption, features important for use in remote locations. Our continued development of diode laser CRDS may impact these areas in addition to thermal or combustion system monitoring.

Work Accomplished

The final vacuum system and pulsed valve designs for the supersonic expansion-cavity ringdown system were finalized during this quarter based on the calculated gas load from the valve. Calculations

were carried out to finalize the pumping speed specifications for the system diffusion pump required to maintain the baseline operating pressure during pulsed valve operation. With the help of Harald Oser of SRI, a commercial source for the slit-jet valve has been identified. Pulsed valve and vacuum components were ordered, and system construction will begin as the required components arrive. Work has been initiated toward construction of a frame for mounting the vacuum system that will house the slit-jet valve. Assembly of the system will begin upon the arrival of the major components. This system will initially be tested using volatile organic compounds and ultimately will be evaluated for dioxin-monitoring applications.

Experiments continue for evaluating the use of the diode laser cavity ringdown system (DL-CRDS) for VOC detection. Unfortunately, after initial very promising results for chlorobenzene were obtained, the external cavity diode laser (ECDL) system began to experience excessive mode-hops (discontinuous frequency shifts). Therefore experiments are continuing using the distributed feedback (DFB) laser. Although the DL-CRDS system is operating well, the DFB does not provide significant tuning range, preventing us from tuning to the absorption maximum of the species of interest. However, although the final system sensitivity can not be determined in this fashion, the general response of the system for different compounds can be evaluated. Work on the DL-CRDS system has focused on improving the reproducibility of VOC measurements. A new absolute pressure gauge operating at a lower pressure was installed to compare with previous measurements made using a higher pressure gauge combined with the volume ratio method. The results from both methods thus far are in good agreement for chlorobenzene.

Work Planned

The primary components for the slit-jet expansion system are anticipated to arrive this quarter. Significant effort will be required to construct the unit once all components have arrived. It is expected

that the vacuum system will be assembled by the end of the next quarter for testing to begin in the fall.

For the DL-CRDS work, we will focus on optimizing the reproducibility of the system and evaluating the system performance for additional VOCs. To date we have data for chlorobenzene, benzene, and toluene and expect to obtain data for dichloro- and trichloro-ethylene in the near future. The ECDL failure is a delay, but we can continue to see how the system responds at the DFB wavelength to various compounds. Different compounds sometimes respond differently in the vacuum system. This type of evaluation can continue using the DFB, and may ultimately prove to be more important than being able to tune to the exact maximum absorption wavelength. A variable temperature control will be added to the vacuum cell to evaluate analyte adsorption onto the cell walls or mirror surfaces. After repair, the ECDL will be reinstalled in the system. Design of a membrane separation system to allow for VOC analysis in water will also begin.

References

43. R. Zimmerman, J.J. Heger, M. Blumenstock, R. Dorfner, K-W. Schramm, U. Boesl, and A. Kettrup. 1999. On-line measurement of chlorobenzene in waste incineration flue gas as a surrogate for the emission of polychlorinated dibenzo-p-dioxins/furans (I-TEQ) using mobile resonance laser ionization time-of-flight mass spectrometry. *Rapid Communication Mass Spectrometry* 13:307-314.

44. For example,

J.J. Scherer, J.B. Paul, A. O'Keefe, and R.J. Saykally. 1997. Cavity ringdown laser absorption spectroscopy: history, development, and application to pulsed molecular beams. *Chemical Reviews* 97:1:25-51.

G.P. Miller and C.B. Winstead. 2000. Cavity ringdown laser absorption spectroscopy. In *Encyclopedia of Analytical Chemistry*, R.A. Meyers, ed. Chichester, England: John Wiley and Sons, Ltd. pp. 10734-10750.

45. K. Liu, R. S. Fellers, M.R. Viant, R.P. McLaughlin, M.G. Brown, and R.J. Saykally. 1996. A long path length pulsed slit valve appropriate for high temperature operation: infrared spectroscopy of jet-cooled large water clusters and nucleotide bases. *Review of Scientific Instruments* 67:2:410.

46. N.B. French, B.K. Gullet, H. Oser, H-H. Grotheer, D. Natschke. 1997. Joint DOE/EPA jet-REMPI dioxin CEM test. Final Report.

47. Department of Energy. September 2000. Subsurface barrier verification with the SEAtrace™ monitoring system. U.S. Department of Energy Innovative Technology Summary Report DOE/EM-0549.